ROYAL SOCIETY OF CHEMISTRY

FEATURE ARTICLE

CrossMark
click for updates

Thin films and nanostructures of niobium pentoxide: fundamental properties, synthesis methods and applications

Rozina Abdul Rani,*[a] Ahmad Sabirin Zoolfakar,[ab] Anthony P. O'Mullane,[c] Michael W. Austin[a] and Kourosh Kalantar-Zadeh*[a]

As one of the transition metal oxides, niobium pentoxide (Nb_2O_5) offers a broad variety of properties that make it a potentially useful and highly applicable material in many different areas. In comparison to many other transition metal oxides, Nb_2O_5 has received relatively little attention, which presents a significant opportunity for future investigations aimed at fundamentally understanding this material and finding new and interesting applications for it. In this article, a general overview of Nb_2O_5 is presented which focuses on its fundamental properties, synthesis methods and recent applications, along with a discussion on future research directions relevant to this material.

[a]School of Electrical and Computer Engineering, RMIT University, Melbourne, VIC 3001, Australia. E-mail: rozina.abdulrani@student.rmit.edu.au; kourosh.kalantar@rmit.edu.au

[b]Faculty of Electrical Engineering, Universiti Teknologi MARA, 40450 Shah Alam, Malaysia

[c]School of Chemistry, Physics and Mechanical Engineering, Queensland University of Technology, GPO Box 2434, Brisbane, QLD, 4001, Australia

1. Introduction

Niobium pentoxide (Nb_2O_5) is a metal oxide with great potential but to date this has yet to be fully realized. Interest in Nb_2O_5 can be dated back to the early 1940s when the polymorphs of Nb_2O_5 were first studied.[1,2] Nb_2O_5 has many polymorphic forms which gives rise to an interesting series of structural phases. The phases are generally based on NbO_6 octahedral groups, forming various configurations from the rectangular blocks or columns.[3] Nb_2O_5 is relatively abundant in nature and has high corrosion resistance as well as being thermodynamically stable.[4–6]

In the very early stages of research on Nb_2O_5, this material was mostly studied in bulk or thin layer forms as well as in suspensions.[7–9] The very first applications of Nb_2O_5, as a functional material, were investigated as catalysts, sensors and in electrochromism.[10–17] The unique performance of Nb_2O_5 in such studies was due to an understanding of its energy band diagram and the identification of crystal phases, which created the initial interest among researchers to explore more of this metal oxide's capabilities. Nb_2O_5 has grown in popularity in recent years and a variety of morphologies ranging from large

Rozina Abdul Rani received her Bachelor of Engineering (Electrical and Electronic) with Honours (2001) and Master of Science (2007) degree from Universiti Sains Malaysia, Malaysia. She is currently undertaking her candidature for a PhD at RMIT University. Previously, she has been working as a senior researcher at MIMOS Berhad. Her research interests include synthesis and characterization of nanostructured metal oxides, dye-sensitized solar cells, chemical sensors and batteries.

Ahmad Sabirin Zoolfakar received his B. Eng. (Electrical) with Honours from Universiti Malaya, Malaysia (2001), MSc (Microelectronic Systems and Telecommunications) from The University of Liverpool, United Kingdom (2003) and PhD at RMIT University, Australia (2014). He is a senior lecturer in the Faculty of Electrical Engineering at Universiti Teknologi MARA. His research interests include aqueous chemical synthesis, gas vapour synthesis, nanotechnology and materials science. At present the prime focus of his work concerns metal oxide for application in sensor development.

This journal is © The Royal Society of Chemistry 2014

J. Mater. Chem. A, 2014, **2**, 15683–15703 | 15683

size bulk crystals to different nanostructures have been reported.[18–25] In particular, nanostructured Nb_2O_5 offers high surface to volume ratios and quantum confinement effects that enable unique physical and chemical interactions to occur at the surface. As a result, such morphological manipulations significantly influence the optical and electronic properties of Nb_2O_5 leading to unique observations that are not seen in its bulk forms. Similarly, the chemical and physical properties of Nb_2O_5 can also be modified *via* other routes such as the incorporation of foreign ions, alteration of the crystal phase and post synthesis heat treatment.[26–28]

More recently, attention on Nb_2O_5 has gained more momentum due to applications other than electrochromism

and catalysis. Especially, thin films and nanostructured Nb_2O_5 have been utilized in batteries, solar cells and other electronic devices such as memristors.[20,29–31] However, most of these investigations are still in their infancy and much more research should be conducted to explore the true capabilities of Nb_2O_5 in these and other applications. Thus, more comprehensive studies on Nb_2O_5 should be conducted to provide further insight for researchers who intend to use this material for such applications.

In this review article, we present a broad review on Nb_2O_5 that includes its fundamental properties, synthesis methods and applications. Many of the common methods for synthesizing thin films and nanostructures of Nb_2O_5 are presented with a separate emphasis on liquid and vapour phase techniques. We summarize a selection of interesting applications that exploit Nb_2O_5 as the core material. In the final section, future outlooks on the possibilities to expand the areas of research and investigations using this material are elucidated.

2. Fundamental properties

In the following section, an overview of the basic properties of Nb_2O_5 including crystal structure, electronic band diagram and electrical properties are presented. The fundamentals of the optical, mechanical and thermal properties of Nb_2O_5 are also discussed.

2.1 Crystal structure

Nb_2O_5 is a transparent (due to its large band gap), air-stable and water-insoluble solid material with a relatively complicated structure that displays extensive polymorphism.[32] There are almost 15 polymorphic forms of Nb_2O_5 that have so far been reported, however, the most common crystal phases are generally pseudohexagonal (TT-Nb_2O_5), orthorhombic (T-Nb_2O_5), and monoclinic (H-Nb_2O_5).[3,27,32,33] As shown in Fig. 1,

Dr Anthony O'Mullane is an Australian Research Council Future Fellow and Senior Lecturer at Queensland University of Technology (Australia). He received his PhD degree (2001) from University College Cork (Ireland) and completed post-doctoral fellowships at Technische Universitat Darmstadt (Germany), the University of Warwick (UK), and Monash University (Australia). He previously held a position (2008) at RMIT University (Australia) until moving to QUT in 2013. Dr O'Mullane's research interests are the electrochemical synthesis and characterisation of nanostructured materials; electrocatalysis; catalysis; semi-conducting charge transfer complexes; Li batteries; and the application of electrochemical methods to various aspects of physical, chemical and biological science.

Michael Austin received his PhD degree in electronic engineering from the University of London, London, U.K., in 1982. Since then he has been a member of academic staff, and a Professor since 1996, in what is now known as the School of Electrical and Computer Engineering at RMIT University, Melbourne, Australia. He was the Director of RMIT's Microelectronics and Materials Technology Centre from 1994 to 2012 and is currently leader of the Functional Materials for Advanced Devices project in RMIT's Platform Technologies Research Institute. Professor Austin has over 30 years' experience in micro/nano fabrication technologies and their application in device fabrication.

Kourosh Kalantar-Zadeh is a Professor at RMIT University, Australia. He received his BSc (1993) and MSc (1997) degrees at Sharif University of Technology, Iran, and Tehran University, Iran, respectively, and PhD at RMIT University, Australia (2002). His research interests include chemical and biochemical sensors, nanotechnology, microsystems, materials science, electronic circuits, and microfluidics. Prof Kalantar-Zadeh is the Director of Centre for Advanced Electronics and Sensors (CADES) at RMIT University and the author of approximately 300 peer reviewed scientific papers and books. Prof Kalantar-Zadeh is internationally recognized for his research on nanotechnology enabled sensors and two dimensional semiconductors.
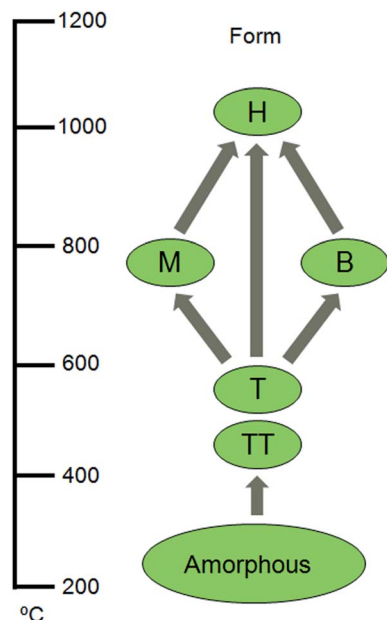
Fig. 1 (a) Alteration of Nb_2O_5 crystal phase as a function of temperature. Reprinted with permission from ref. 34. Copyright 1990, Elsevier.

after any relatively low temperature synthesis route amorphous Nb_2O_5 is normally obtained and then crystallizes at ~500 °C into TT or T phases, at medium-temperature (~800 °C) transforms into the M phase (tetragonal), and above ~1000 °C it forms the H phase.[34] Despite this general temperature effect, the method of preparation, the nature of the starting material and the presence of impurities as well as interactions with other components also play decisive roles in the formation of the resulting Nb_2O_5 crystal.[3,34] $H\text{-}Nb_2O_5$ is the most thermodynamically stable crystal phase and is always produced when heated to temperatures above 1000 °C, while the TT- and $M\text{-}Nb_2O_5$ forms are mostly metastable.[3,35] It is important to mention that in some reports, Nb_2O_5 crystal phases have been re-designated as $\gamma = T$, $\beta = M$, and $\alpha = H$.[32] However, there are still many inconsistencies regarding the identification of Nb_2O_5 crystal phases. Some investigators suggested that the M is simply disordered H phases[34] whereas $M\text{-}Nb_2O_5$ has been reported as a tetragonal Nb_2O_5 phase by Mertin et al.[35]

Some of the crystallographic properties of the different crystal phases of Nb_2O_5, with reference to their associated literature, are presented in Table 1. The unit cells of TT-, T- and $H\text{-}Nb_2O_5$ crystals are shown in Fig. 2. A unit cell of $TT\text{-}Nb_2O_5$

contains half of the formula equivalent with a constitutional defect of an oxygen atom per unit cell (Fig. 2a).[36] Each niobium (Nb) atom is at the center of four, five or six oxygen atoms on the ab-plane and an Nb–O–Nb–O chain structure exists along the c-axis. As a result, the oxygen deficiency leads to the distortion of these polyhedra. Meanwhile, the $T\text{-}Nb_2O_5$ phase is constructed with the orthorhombic unit cell where each Nb atom is surrounded by six or seven oxygen atoms, creating distorted octahedra or pentagonal bipyramids (Fig. 2b and d).[36,37] The polyhedra are connected by edge- or corner-sharing in the ab-plane and by corner-sharing along the c-axis.[36] The TT and T phases of Nb_2O_5 have quite similar X-ray diffraction patterns where the main difference is that some reflections that are split in $T\text{-}Nb_2O_5$ occur as one peak in the XRD patterns of the $TT\text{-}Nb_2O_5$ phase.[32,34] The broadening of peaks in TT (or the splitting of the corresponding peaks in T) is due to the occupancy of niobium atoms in separate, but closely-spaced, equivalent sites in the T form, giving rise to the split peaks observed from certain reflections, and the ability of Nb to occupy either of these sites or places between the TT form, resulting in broadening of the same peaks in XRD patterns of TT.[34] These observations suggest that $TT\text{-}Nb_2O_5$ is a less crystalline form of $T\text{-}Nb_2O_5$, stabilized by impurities such as OH^-, Cl^-, or oxygen vacancies.[34] The monoclinic lattice of $H\text{-}Nb_2O_5$ contains ReO_3 type blocks of 3×4 and 3×5 groups containing NbO_6 octahedra (Fig. 2c and e).[36,38,39] These blocks are coupled by edge-sharing with a shift of half a unit cell dimension along the c-axis. NbO_6 units are connected by corner-sharing with each other within a block.[36] One of the 28 Nb atoms in each unit cell is present in a tetrahedral site, which occurs at some block junctions.[32,40] $M\text{-}Nb_2O_5$ has similarity with the $H\text{-}Nb_2O_5$ crystal structure, which contains 4×4 of ReO_3 type blocks.[3,35] This was concluded from the close relationship of the X-ray powder diagram of the M- and H-forms, which agree in a large number of reflections.[3]

2.2 Band energy diagram and electrical properties

In electronic device development based on metal oxides, several properties of the incorporated materials are of utmost importance. These include the band energy diagram, electrical conductivity and dielectric permittivity. Nb_2O_5 is a wide band gap n-type semiconductor with a conduction band comprised of empty Nb^{5+} 4d orbitals and has a conduction band value that is 0.2–0.4 eV higher than titanium dioxide (TiO_2).[41] Its band gap energy (E_g) values have been reported to be in the order of 3.1 (semiconducting) to 5.3 eV (insulating with conductivity of

Table 1 Lattice parameters of TT, T, M and H phases of Nb_2O_5

Crystal phase	Space group	Lattice constant			Temperature (°C)	Refs
		a (Å)	b (Å)	c (Å)		
Pseudohexagonal	P6/mmm	3.60	3.61	3.92	500	27,51 and 52
Orthorhombic	Pbam	6.19	3.625	3.94	—	51,53 and 54
Tetragonal	I4/mmm	20.44	3.83	3.82	900	35 and 55
Monoclinic $\beta = 119.9° \pm 0.4°$	P12/m1, P2, P2/m	21.14	3.82	19.45	>1000	1,3,27,53,and 56–58

This journal is © The Royal Society of Chemistry 2014

J. Mater. Chem. A, 2014, **2**, 15683–15703 | **15685**
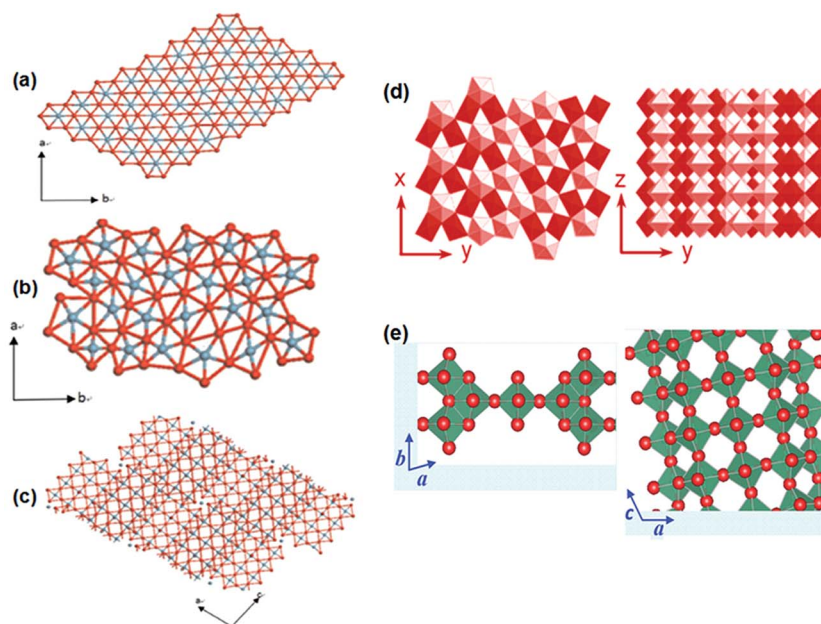
Fig. 2 Atomic representation of (a) pseudohexagonal (TT-Nb$_2$O$_5$), (b) orthorhombic (T-Nb$_2$O$_5$), (c) monoclinic (H-Nb$_2$O$_5$) and 3D structure schematics of (d) orthorhombic (T-Nb$_2$O$_5$) and (e) monoclinic (H−Nb$_2$O$_5$). (a–c) Reprinted with permission from ref. 36. Copyright 2012, Co-Action Publishing, (d) reprinted with permission from ref. 37. Copyright 2007, American Chemical Society, (e) reprinted with permission from ref. 38. Copyright 2012, WILEY-VCH Verlag GmbH & Co. KGaA, Weinheim.

$\sigma = \sim 3 \times 10^{-6}$ S cm^{-1}).[42–44] The ability to tune the band gap of Nb$_2$O$_5$ is possible and factors such as stoichiometry, crystallinity, heat treatment and incorporated foreign ions can dramatically influence the band gap energy. Previous studies have also shown that decreasing the dimensions of Nb$_2$O$_5$ into the nanoscale results in a blue shift of the energy gap, which can be attributed to the quantum-size effect.[45] Significantly, nanostructured Nb$_2$O$_5$ possesses grain dimensions that can critically influence the electronic structure of the material.[46]

Le Viet *et al.* experimentally determined the band gap of crystalline Nb$_2$O$_5$ nanofibers (hexagonal, orthorhombic and monoclinic) which had been sintered at three different temperatures (500, 800 and 1100 °C).[27] Based on the Tauc plots derived from the absorption spectra in Fig. 3a, they found that the hexagonal (labelled as H-Nb$_2$O$_5$), orthorhombic (labelled as O-Nb$_2$O$_5$) and monoclinic (labelled as M-Nb$_2$O$_5$) forms of Nb$_2$O$_5$ exhibited band gaps of 3.85, 3.77 and 3.79 eV, respectively.[27] Meanwhile, Abe reported that the powder-synthesized orthorhombic Nb$_2$O$_5$ had a band gap value of 3.4 eV, while that of monoclinic Nb$_2$O$_5$ gave a reported value of 3.1 eV.[26] Moreover, the same author also investigated the effect of doping on the energy band gap of Nb$_2$O$_5$ by incorporating different concentrations of germanium (Ge) in the monoclinic Nb$_2$O$_5$ films. The optical absorption edge of the monoclinic Nb$_2$O$_5$ which is derived using the Kubelka–Munk function was observed at 3.1 eV without Ge doping which shifted up to 3.35 eV as the Ge concentration was increased.[26] The incorporation of tungsten and molybdenum into Nb$_2$O$_5$ has also been reported as well as the treatment of Nb$_2$O$_5$ with hydrogen peroxide in order to manipulate the band gap of Nb$_2$O$_5$.[47]

Recently, Liu *et al.* fabricated single-crystalline nanoporous Nb$_2$O$_5$ nanotubes using a two-step solution route; the growth of uniform single-crystalline Nb$_2$O$_5$ nanorods and the following ion-assisted selective dissolution along the [001] direction.[48] The band gap of Nb$_2$O$_5$ nanotubes and nanorods are 3.97 and 3.72 eV, respectively (Fig. 3b). As mentioned previously, the 0.25 eV difference was due to the blue shift of the absorption edge for the porous nanotubes compared to solid nanorods which is due to the quantum size effect in hollow Nb$_2$O$_5$ nanotubes.[48] The same effect was also observed by Brayner *et al.* in the transmission spectrum of Nb$_2$O$_5$ particles: a significant blue shift of the absorption edge was observed and therefore the band gap increased from 3.4 eV to 4.2 eV, as the particle size of Nb$_2$O$_5$ decreased from about 40.0 nm to 4.5 nm.[49] The effect of grain size on the band gap of Nb$_2$O$_5$ was also presented by Agarwal *et al.*,[50] although they suggested that the energy of the absorption edge is influenced by both the size and local coordination of the grains.

In Nb$_2$O$_5$, like other semiconductors, the concentration of charge carriers is directly related to the defect structure of the metal oxide which is dependent on temperature and oxygen pressure.[59] Greener *et al.* conducted a detailed analysis of the relation between conductivity of α-Nb$_2$O$_5$ (monoclinic) and temperature under ambient oxygen pressure.[60] As presented in Fig. 4, they showed that an increase in temperature and decrease in oxygen partial pressure increased the conductivity of α-Nb$_2$O$_5$. These results are in excellent agreement with the measurements by Kofstad and Chen *et al.*[61,62]

To scale down the physical dimensions of integrated circuits, investigating of high-κ (high permittivity) materials is important for reducing the leakage current in integrated
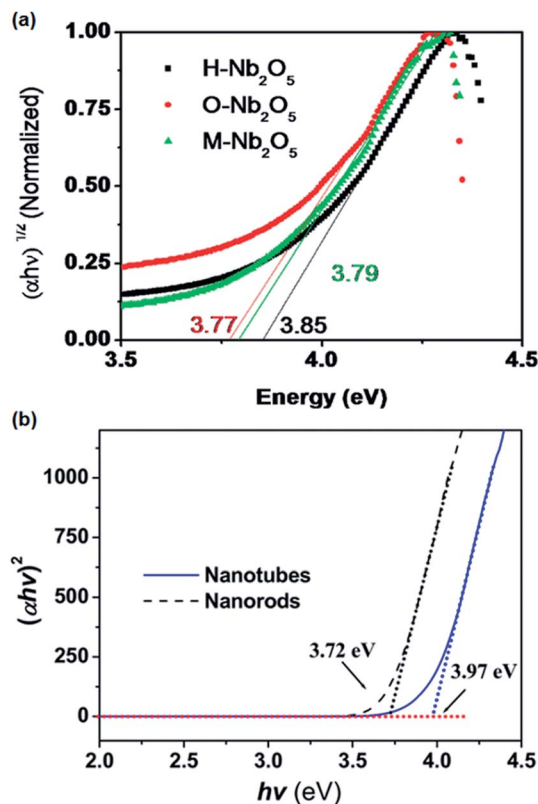
15686 | *J. Mater. Chem. A*, 2014, **2**, 15683–15703

This journal is © The Royal Society of Chemistry 2014

Fig. 3 Tauc plot of $(\alpha h v)^2$ vs. photon energy (hv) of (a) hexagonal, orthorhombic and monoclinic Nb_2O_5 nanofibers, (b) orthorhombic Nb_2O_5 nanorods and nanotubes measured at room temperature. α is defined as absorption the coefficient. (a) Reprinted with permission from ref. 27. Copyright 2010, American Chemical Society, (b) reprinted with permission from ref. 48. Copyright 2011, Springer.

capacitors and gate insulators. Based on experimental measurements and first-principles calculations, Clima et al. reported that the relative dielectric permittivity of sol–gel deposited Nb_2O_5 to be 77 for the orthorhombic phase, 58 for the δ_A-hexagonal phase and 38 for the δ_B-hexagonal phase.[63] They found that the dielectric constant of Nb_2O_5 strongly depended on the crystal structure and the inspection of the permittivity tensors revealed that the dielectric constants are anisotropic. More recently, Nb_2O_5 thin films were grown by atomic layer deposition using novel precursor chemistry for metal–insulator–metal (MIM) capacitors with a relative permittivity of 28.[64] However, after annealing at 650 °C, the films' relative permittivity values increased to 45–50 due to the enhanced crystallinity of the films. In addition, Cavigliasso et al. reported that the dielectric constant of Nb_2O_5 films created electrochemically by electrooxidation depended on the electrolyte used, and resulted in dielectric constant values over the range of 49 to 120.[65]

Electronic mobility is another important parameter in semiconductor device development especially for field effect transistors (FETs). A mobility value of 7×10^{-2} cm^2 V^{-1} s^{-1} for α-Nb_2O_5 at a temperature of 1200 °C was reported by Yahia.[66] Further, it has been shown that the mobility is increased by increasing the temperature.
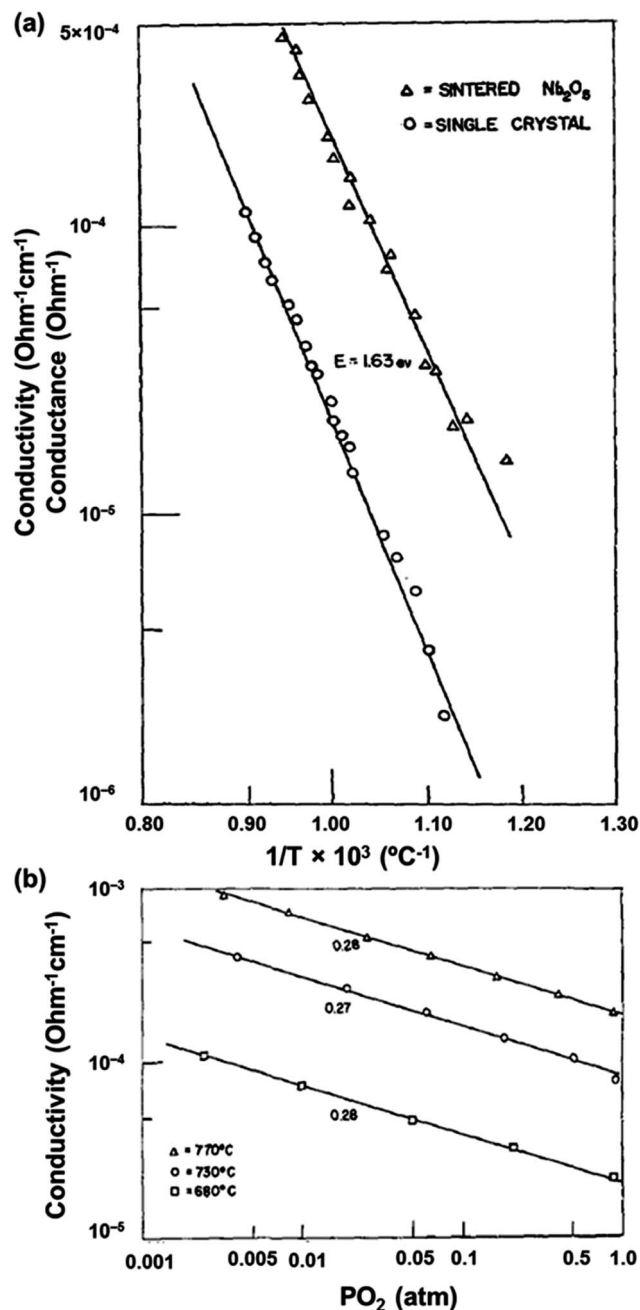

Fig. 4 (a) Electrical conductivity of sintered α-Nb_2O_5 and electrical conductance of Nb_2O_5 single crystal versus $1/T$ for specimens heated in air. (b) Electrical conductivity of sintered α-Nb_2O_5 versus oxygen partial pressure. Reprinted with permission from ref. 60. Copyright 1961, AIP Publishing LLC.

2.3 Optical properties

As mentioned in Section 2.2 the band gap of Nb_2O_5 ranges between 3.1 and 5.3 eV. As a result, Nb_2O_5, depending on its crystallinity and grain morphology can efficiently absorb light in the near UV and UV regions of the spectrum or it can be used as a transparent material to UV light. Nb_2O_5 has been identified as being capable of reversible and rapid coloration in the presence of intercalating ions such H^+ and Li^+ ions. It has been

This journal is © The Royal Society of Chemistry 2014

J. Mater. Chem. A, 2014, 2, 15683–15703 | 15687

reported that this phenomenon can modulate the Nb_2O_5 optical transmission from a quasi-transparent state ($T \sim 85\%$) to less than $T \sim 10\%$ in the ultraviolet (UV), visible or near infrared (IR) range, and can exhibit either a blue or brown colour depending on the crystallinity of the film.[17,67–69]

The optical properties of Nb_2O_5 have been experimentally studied via various techniques such as spectrophotometry and spectroscopic ellipsometry.[70–73] The refractive index value of Nb_2O_5 films has been reported to be in the order of 2 to 2.3.[71,73] Also the crystallinity of the film plays a significant contribution to the refractive index of the material as it decreases from 2.30 to 2.20 after being annealed from room temperature to 700 °C.[70]

2.4 Mechanical properties

Besides electronic and optical properties, an investigation of the mechanical properties of Nb_2O_5 is also of major importance for the fabrication of electronic devices especially for the development of flexible mechanical devices and actuators such as micro electro-mechanical system (MEMS) devices. Stress or strain commonly occurs in thin films depending on the deposition process and constraints imposed by the substrate. The average hardness (H) and Young's modulus (E_r) values of as-sputtered Nb_2O_5 films have been reported to be in the order of 5.6 to 6.8 GPa and 117 to 268 GPa respectively, which is again influenced by the crystal phase.[70,74]

In flexible device applications, the bending test is essential to perform in order to monitor the effects of stretching on the device output and to make sure that all the component layers are stable even after several thousand flexes. Some of the appropriate flexibility tests and other related mechanical tests for electronic devices have been described in detail elsewhere.[75–78] Hota et al. have demonstrated that sputtered Nb_2O_5 thin films ($\sim$50 nm thickness) on flexible polyethylene terephthalate (PET) substrates show high mechanical flexibility in a repetitive bending test.[79] A collapsing radius test, which is one of the common bending test techniques, was applied to MIM capacitors based on sputtered Nb_2O_5 thin films, and the obtained results show endurance of up to 2500 flexes.

2.5 Thermal properties

In an electronic system, heat dissipation is an acute problem due to miniaturization and the increasing power of microelectronic circuits. Thus, thermal conductor materials with high thermal conductivity and a low coefficient of thermal expansion (CTE) are essential for the purpose of heating and cooling. For Nb_2O_5, a limited number of studies have been carried out on its thermal properties. An investigation of the high-temperature thermal expansion of monoclinic Nb_2O_5 was conducted using X-ray and dilatometric techniques by Manning et al.[80] The results revealed that the lattice thermal expansion of Nb_2O_5 is anisotropic where the mean coefficients in the a, b, and c directions were 5.3×10^{-6}, 0 and 5.9×10^{-6} per °C, respectively. Previous works also demonstrated the low thermal expansion behaviour of Nb_2O_5 over the temperature range of 20 to 1000 °C.[81,82] In addition, another report demonstrated a negative thermal expansion of Nb_2O_5 at relatively high

temperatures as large as 500 °C (ref. 83 and 84) which was attributed to the recombination of the microcrack network formed during cooling. There are just a few reports regarding the Seebeck coefficient of Nb_2O_5.[85] It has been reported that its Seebeck coefficient changes from -0.5 to -1.2 mV per °C when the temperature changes from 500 to 1000 °C.

3. Synthesis of Nb_2O_5

Nb_2O_5 has been synthesized using many approaches and the key motivation in choosing the right synthesis method is its capability in tuning the properties of Nb_2O_5 (mostly crystal phase and morphology). In this section, we have chosen the most common synthesis methods and classified them into two major categories: liquid and vapour phase based. In addition, complementary methods are also presented.

3.1 Liquid phase deposition methods

Liquid phase techniques include methods such as hydrothermal, anodization, sol–gel and electrodeposition. These methods are chosen due to their low capital cost, relatively low operating temperatures and high control over Nb_2O_5's properties in comparison to vapour phase deposition techniques, which is crucial for the fabrication of cheap and low-heat-tolerant substrates.

3.1.1 Hydrothermal and solvothermal methods. Hydrothermal (in water) and solvothermal (in other solvents such as acetone and isopropyl alcohol) synthesis techniques are simple methods that have been utilized to produce metal oxide crystals. These methods involve an ionic source of metal in a solution which is heated at an elevated temperature for a certain period of time. For the deposition of Nb_2O_5, the solution of Nb^{5+} ions is sourced either via the interaction of niobium metal in an acid or base or the dissolution of a niobium salt such as niobium chloride, niobium ethoxide, or ammonium niobium oxalate (see Table 2). The solvents are then heated at a temperature in the range of 100–600 °C for duration of a few hours to several days (see Table 2). Normally, this process allows the nucleation and growth of naturally crystalline Nb_2O_5 to proceed. Nanostructured Nb_2O_5 such as nanorods, nanobelts, nanospheres and other configurations are also possible to be synthesized using these hydrothermal or solvothermal methods. A brief summary of the type of nanostructured Nb_2O_5 that can result from such methods is presented in Table 2. Fig. 5 presents a selection of the type of Nb_2O_5 nanostructures that have been achieved using a few selected hydrothermal or solvothermal methods. Due to the high-aspect-ratio properties and high surface area that can be obtained, these methods offer great potential for obtaining Nb_2O_5 that can be used in various specific applications including lithium-ion batteries, dye-sensitized solar cells and photocatalysis applications which will be explained in the later sections.[38,86–89]

3.1.2 Anodization method. Anodization is one of the most widespread nano-fabrication methods due to its capability of forming highly porous and ordered oxide morphologies.[90,91] In a typical anodization experiment, a potential is applied between

15688 | J. Mater. Chem. A, 2014, 2, 15683–15703

This journal is © The Royal Society of Chemistry 2014

Table 2 Summary of Nb_2O_5 nanostructures obtained using hydrothermal and solvothermal processes and their synthesis conditions

Morphology	Dimension (nm)	Solution	Temperature (°C)	Duration (h)	Crystal phase
Nanograins, nanorods and nanoplatelets[164]	D: 50–80, L: >1000	$NbCl_5$ and ethanol in cyclohexanol	200–240	8–90	Orthorhombic for T > 225 °C
Nanoparticles[165]	D: 18–35	$NbCl_5$ in anhydrous benzyl alcohol	250	72	Pseudohexagonal
Nanopowder[166]	L: < 80	Niobium pentabutoxide in toluene	300	2	Pseudohexagonal
Nanobelts[167]	T: ∼ 15, W: ∼60	Nb powder in urea	170–200	24–336	N/A
Nanocables and nanorods[168]	D: 50–80, L: > 1000	$NbCl_5$ and ethanol in cyclohexanol	200–240	8–90	Orthorhombic
Nanorods[169]	D: 50	Nb powder in distilled water	200	72–720	Orthorhombic
Nanosheets[86]	T: 3–5	NbO_2 powder in distilled water and ethanol containing 1 M urea	130	72–720	Orthorhombic and monoclinic
Mesoporous[170]	—	$NbCl_5$ in ethanol mixed with triblock copolymer dissolved in distilled water	110	24	Orthorhombic after calcined at 600 °C
Mesoporous spheres[171]	D: 400–500	Niobium ethoxide, diethylene glycol and acetone in water	180	4–12	Pseudohexagonal
Nanospheres[89]	D: 20–50	Ammonium niobate oxalate hydrate in distilled water	580	1	Pseudohexagonal
Nanorods[89]	D: 5–20, L: 100–500	Ammonium niobate oxylate hydrate and oleic acid in trioctylamine	180	2–6	Pseudohexagonal
Nanotrees[172]	D: 30–500	Lithium hydroxide in HF acid	150–200	20–40	Pseudohexagonal
Nanorods[173]	D: 50–100	Ammonium fluoride	150	24–144	Orthorhombic for duration >48 h
Nanoparticle[88]	D: 9–35	Ammonium niobium oxalate and hydrogen peroxide in distilled water	100–175	2–24	Orthorhombic
Hollow microspheres[174]	D: 1000–2000	Nb_2O_5, LiOH and $NH_3 \cdot H_2O$ in H_2O_2	240	24	Pseudohexagonal after calcined at 500 °C
Nanocomposite[87]	D: 25–29	Ammonium niobate oxalate hydrate, sucrose and HCl in deionized water	180	12	Pseudohexagonal
Nanorods[38]	D: 22, L: 230	$NbCl_5$ in HCl	210	24	Monoclinic after calcined at 450 °C

two electrodes; a working and counter electrode, which are both immersed in a liquid electrolyte. An electrical current or voltage is then applied, which results in electrochemical reactions occurring on the surface of the metal electrode (working electrode) and an oxide film is formed. The growth and morphology of the anodic oxide film strongly depends on the applied anodization potential, the composition of the electrolyte (aqueous, organic solvent with or without water and etching agent content), the electrolyte temperature, and the anodization duration. The as-anodized Nb_2O_5 films are mainly amorphous and require a post-annealing treatment to be converted into highly crystalline and stoichiometric Nb_2O_5.

Studies on anodic Nb_2O_5 films have been conducted as early as the 1960s. Draper et al. presented work that was undertaken to study the anomalies in published work on the structure of the anodic films formed on niobium (Nb) and how the physical

nature of the film material might influence the growth rate.[92] Later, a study on anodic Nb_2O_5 film properties (i.e., resistivity, dielectric constant) was presented by Wood et al.[93] Other early studies on anodized Nb_2O_5 surface morphology and crystallization analysis using an electron microscope, electron-beam crystallization and reflection electron diffraction have been reported elsewhere.[94,95]

The anodization of Nb has been intensively studied in various electrolytes (sulfuric acid, phosphoric acid, NaOH, Na_2CO_3, HF, glycerol, ethylene glycol, fluoride, and phosphorus based solutions). Most of the reported anodic Nb_2O_5 films consist of highly nanoporous structures on a Nb foil substrate.[96–103] In one of the most important reports, conducted by Habazaki et al., the effect of water content on the formation of porous Nb_2O_5 anodized in a K_2HPO_4–glycerol electrolyte as well as at elevated temperature was discussed.[96] They showed

This journal is © The Royal Society of Chemistry 2014

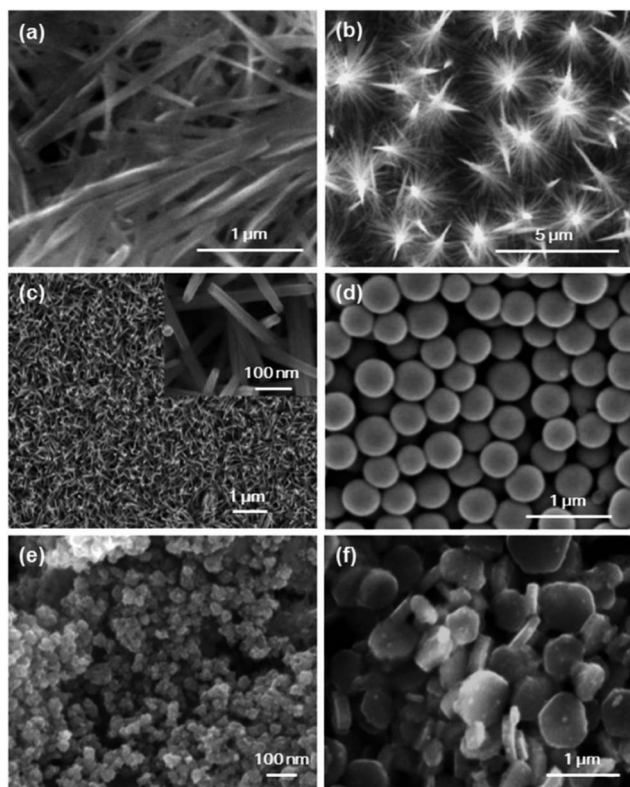J. Mater. Chem. A, 2014, **2**, 15683–15703 | **15689**

Fig. 5 Scanning electron microscopy (SEM) images show the morphologies of the hydrothermally synthesized Nb_2O_5. (a) Nb_2O_5-nanosheets synthesized from NbO_2 precursor at 130 °C for 30 days, (b) Nb_2O_5-nanotrees synthesized from niobium foil dipped in HF acid solution and lithium hydroxide of pH = 3.3–3.4 at 150–200 °C for 20–40 h, (c) Nb_2O_5-nanorods synthesized at 150 °C for 48 h in NH_4F aqueous solution of 0.02 M concentration, (d) Nb_2O_5-mesoporous spheres synthesized using niobium ethoxide mixed with DEG solvent and acetone at 180 °C for 12 h, (e) Nb_2O_5-nanoparticles synthesized in ammonium niobium oxalate using a mix of distilled water and hydrogen peroxide kept at 100 °C for 12 h and (f) Nb_2O_5-hexagonal nanoplatelets synthesized in a mix of $NbCl_5$ in ethanol at pH = 2.1 kept at a temperature of 235 °C for 90 h. (a) Reprinted with permission from ref. 86. Copyright 2010, Elsevier, (b) reprinted with permission from ref. 172. Copyright 2010, IOP Publishing Ltd., (c) reprinted with permission from ref. 173. Copyright 2011, Elsevier, (d) reprinted with permission from ref. 171. Copyright 2012, WILEY-VCH Verlag GmbH & Co. KGaA, Weinheim, (e) reprinted with permission from ref. 88. Copyright 2014, Elsevier, (f) reprinted with permission from ref. 164. Copyright 2009, Springer.

that by reducing the water content to 0.08 mass%, the porous film growth rate markedly increased (as thick as 28 μm) at 160 °C, which is associated with the increased field strength by a higher concentration of phosphorus species. Ou *et al.* later reported the creation of a three dimensional (3D) vein-like nanostructured network in an electrolyte consisting of ethylene glycol with NH_4F and small content of water (~4%) (Fig. 6a).[23] In all of these processes, an elevated temperature was applied based on the hypothesis that it increases the ion diffusion rate during the anodization process.

Apart from a nanoporous structure, microcones were also obtained by Nb anodization in an electrolyte containing
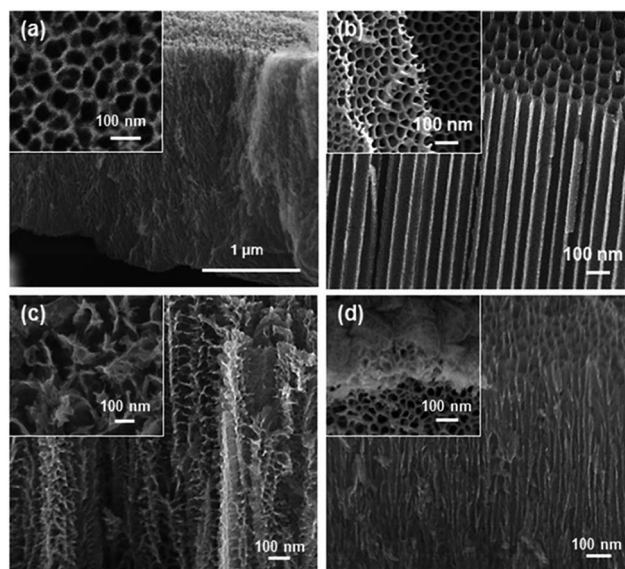

Fig. 6 SEM images of: (a) Nb_2O_5 vein-like nanostructured networks and (b) Nb_2O_5 nanochannelled structure on foil; (c) nanoporous Nb_2O_5 and (d) nanochannelled Nb_2O_5 on FTO (the insets are top view images of the anodic films). (a) Reprinted with permission from ref. 23. Copyright 2012, American Chemical Society, (b) reprinted with permission from ref. 22. Copyright 2014, Elsevier, (c and d) reprinted with permission from ref. 110. Copyright 2013, The Royal Society of Chemistry.

deionized water with a low concentration of HF or in a glycerol electrolyte containing K_2HPO_4.[104–107] Wei *et al.* reported anodized nanotubes of Nb_2O_5 up to 4 μm thick by optimizing the anodization of Nb in an NH_4F based glycerol electrolyte.[108] Recently, Lee *et al.* reported the first anodization procedure to produce highly ordered nanochannels of Nb_2O_5 grown in glycerol containing K_2HPO_4 electrolyte also at 180 °C.[109] They showed that the channel length could be adjusted from a few hundred nm to several tens of μm. Lee *et al.* were successful in growing films of thick nanochannels of Nb_2O_5 by pre-heating the electrolyte at 200 °C before conducting the anodization in order to reduce the water content.[109] Other reports on anodic nanochannelled Nb_2O_5 films were also reported by Abdul Rani *et al.* (Fig. 6b).[22] Moreover, reports on nanoporous Nb_2O_5 films and nanochannelled Nb_2O_5 films obtained from anodizing Nb films, which were RF sputtered on fluorine doped tin oxide (FTO) glass substrates, have also been demonstrated recently (Fig. 6c and d).[69,110,111]

3.1.3 Sol–gel methods. The sol–gel process is a simple wet-chemical method that involves the conversion of selected monomers into a colloidal solution (sol). The sol acts as the precursor for the formation of an integrated network (or gel) which can be eventually used for creating discrete particles or connected networks.[112] The deposition of the final oxide films using a sol–gel process is normally conducted by methods such as dip- or spin coating, electrospinning, or drop-casting. Despite its simplicity, there are some limitations as well. The bonding can be weak, resulting in inhomogeneity in subsequent films. There are also certain difficulties in controlling the reaction rate and porosity.[113–115]

15690 | *J. Mater. Chem. A*, 2014, **2**, 15683–15703

This journal is © The Royal Society of Chemistry 2014

The preparation of Nb_2O_5 *via* sol–gel methods was first reported by Alquier *et al.* in 1986.[112,116] The typical precursors used for Nb_2O_5 films synthesised *via* sol–gel processes are quite similar to the hydrothermal or solvothermal methods, containing a mixture of niobium salt and its solvent. The sol–gel Nb_2O_5 films generally require a post-annealing treatment in order to induce crystallinity. Schmitt *et al.* have reported a sol–gel based Nb_2O_5 thin film by dissolving $NbCl_5$ powder in butanol and acetic acid.[68] The Nb_2O_5 films were deposited by dip-coating and then annealed at 400–600 °C to obtain the TT crystal. Similar procedures have also been demonstrated by other researchers using different precursors such as niobium ethoxide and ammonium niobium oxalate.[4,29,67,117–125] As can be seen from Fig. 7a–c, films consisting of nanoparticle structures are normally obtained by dip or spin coating deposition techniques.[121,124] Different structural morphologies of Nb_2O_5 have been demonstrated by Le Viet *et al.* using electrospinning which resulted in Nb_2O_5 nanofibers as shown in Fig. 7d–f.[27] These nanofibers were synthesized from a polymeric solution prepared from polyvinylpyrrolidone (PVP) and niobium ethoxide in ethanol and hydrolyzed using acetic acid.

3.1.4 Electrodeposition. Electrodeposition can be considered as a common method for the fabrication of nanostructured materials in the form of thin films, powders and composites.[126] This process often involves a two electrode configuration immersed in an electrolyte, where a metal oxide film forms at the cathode in contrast to the anodization method described in Section 3.1.2. The aqueous electrolyte used for Nb_2O_5 electrodeposition generally contains niobium ions and hydrogen peroxide (H_2O_2).[127,128]

In one of the very first electrodeposition reports, Zhitomirsky performed electrodeposition by applying a constant current density of 20 mA cm^{-2} at 1 °C for 20 min in an electrolyte mixture of $NbCl_5$ and H_2O_2.[126,127] The produced Nb_2O_5 thin films exhibited microporosity with a thickness of 0.3 μm, were crack free and adhered well to the substrate. Non-aqueous electrolytes can also be used in electrodeposition but they need to have some supporting electrolyte to allow the conduction of current. Kamada *et al.* added 0.01 M iodine (I_2) and bromine (Br_2) into acetone as an electrodeposition electrolyte to obtain Nb_2O_5 films.[25] Although the addition of I_2 into acetone induced anodic oxidation of the metal anode, subsequent electrochemical dissolution and cathodic deposition did not take place. The addition of Br_2 has been found to promote both anodic dissolution and electrodeposition of Nb species.

3.2 Vapour phase deposition

In general, vapour phase deposition is a process to fabricate layers of materials from the condensation of their vaporized sources under favourable environments. There are two major categories of vapour phase deposition: physical vapour deposition (PVD) and chemical vapour deposition (CVD).

3.2.1 Physical vapour deposition (PVD). PVD techniques are used for depositing a wide variety of films with thicknesses which vary from a few angstroms to several millimetres. The deposition of a film is through the evaporation of the precursors into a vapour phase by physical approaches such as ion bombardment, heat, electron beam or laser irradiation followed by the condensation of the vapour phase onto the required substrate.[129,130]

So far, sputtering has been the most reported PVD technique to deposit Nb_2O_5 films. Generally, Nb_2O_5 films can be obtained using direct current (DC)[72,131–136] or radio frequency (RF)[18,132,137–143] sputtering techniques with metallic niobium (Nb)[72,131,133–135,138–142,144–146] or Nb_2O_5 (ref. 18, 137 and 143) targets in the presence of carrier gases such as argon (Ar) in oxygen (O_2) environments. These techniques are capable of producing Nb_2O_5 films or nanostructured forms with preferred dimensions, crystallinity, nanoscale grain sizes and morphologies by controlling the deposition parameters (*i.e.*; pressure, distance between the target and the substrate, substrate temperature, discharge voltage, RF power) during the sputtering process.[147] Post-annealing treatment in a controlled gas environment is usually used to enhance the crystallinity of the sputtered films.
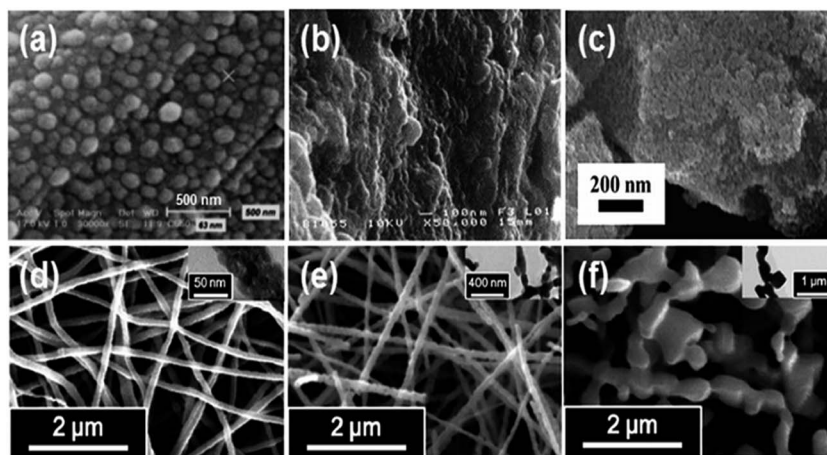

Fig. 7 SEM images of annealed Nb_2O_5 prepared by (a–c) dip-coating sol–gel method and (d–f) electrospinning sol–gel method. (a) Reprinted with permission from ref. 125. Copyright 2012, Springer, (b) reprinted with permission from ref. 121. Copyright 1999, Elsevier, (c) reprinted with permission from ref. 124. Copyright 2012, Elsevier, (d–f) reprinted with permission from ref. 27. Copyright 2010, American Chemical Society.

This journal is © The Royal Society of Chemistry 2014

J. Mater. Chem. A, 2014, **2**, 15683–15703 | **15691**

Even though sputtering can produce high-quality films, this technique is time consuming due to its low deposition rates (typically in the μm per hour range).[148]

In addition to sputtering, other PVD techniques have been established to fabricate Nb_2O_5 films such as ion-beam assisted deposition,[70,71,149,150] thermal evaporation,[151] pulsed magnetron sputtering[145,152] and pulsed laser deposition (PLD).[20,153–155] Pulsed magnetron sputtering and PLD have been found to increase the deposition rate of Nb_2O_5 films to the order of tens of microns per hour and are also able to conserve the original stoichiometry of a bulk target to the deposited film.[148,153] It is also possible to obtain high aspect ratio nanostructures such as nanobundles that have been shown by Ghosh *et al.* using PLD process (Fig. 8).[20]

3.2.2 Chemical vapour deposition (CVD). CVD techniques are also commonly used in the formation of films (in particular conformal coatings) and nanostructures.[156,157] Nb_2O_5 thin films (nanostructured and compact) have been successfully synthesized using CVD techniques such as metal–organic CVD (MOCVD),[158,159] plasma-enhanced CVD (PECVD),[160] atmospheric pressure CVD (APCVD),[161,162] and vapour–liquid–solid (VLS) growth mechanisms under vacuum or atmospheric conditions.[163]

Generally, to deposit the Nb_2O_5 films, precursors such as $NbCl_5$ and pentaethoxy niobium $[Nb(OC_2H_5)_5]$ are transported using reactant/carrier gas species into the reaction chamber, and subsequently decomposed on the surface of a heated substrate.[160]

O'Neill *et al.* showed that the Nb_2O_5 film growth strongly depended on the substrate temperature when deposited by the CVD reaction of $NbCl_5$ with ethyl acetate.[161] At lower temperatures (400–500 °C), the resultant films tended to be uniform,

forming layered growths. Deposition at temperatures higher than 500 °C produced hazy films with fairly uniform columnar nanostructure associated with Volmer–Webber growth throughout the films. At 600 °C a milky appearance was observed, which was attributed to the films being comprised of uniform inter-grown rods that were virtually all aligned perpendicular to the substrate surface. These results indicated that the changes in the morphology of the films with substrate temperature were related to the number of nucleation sites available and the delivery rate of the precursor.[161] In another approach, the initial niobium pentaisopropoxide $[Nb(O^iPr)_5]_2$ precursor was decomposed at 950 °C onto polycrystalline alumina substrates, which resulted in one-dimensional mono-clinic Nb_2O_5 nanorods.[163] Other studies using CVD methods offer excellent alternatives to produce layered Nb_2O_5 especially for fibre coating applications.[158,162]

Furthermore, spray pyrolysis which is a typical aerosol-assisted CVD is among one of the most well utilized methods to synthesis thin or thick Nb_2O_5 films.[19,175–178] This method has the capability of forming large-scale thin films by using a simple apparatus with large productivity. With regard to the substrate temperature, a post annealing treatment is usually required to obtain highly crystalline Nb_2O_5 films if a low temperature is applied during the deposition.

3.3 Thermal oxidation

Thermal oxidation is a simple fabrication technique. The starting material to fabricate Nb_2O_5 is normally Nb metal/foil or powder, and then the thermal oxidation is performed by heating the sample in a furnace at a temperature as high as 1000 °C generally in a O_2 or oxidizing rich environment.[16,21,55,179–183] The technique forces the oxidizing reagent to diffuse into the substrate at a high temperature and react with it. The nanostructured Nb_2O_5 is directly grown onto the surface of a Nb substrate. The resultant structures can vary from compact films to nanowires and core–shell structures. It has been reported that nanowires as long as 20 μm can be produced by this approach.[180,182] The growth of these nanostructures can be controlled by optimizing the temperature, time, metal-catalyst and gas atmosphere during the synthesis process.[184]

4. Applications

Applications of Nb_2O_5 normally involve the utilization of some unique properties of Nb_2O_5 such as its electronic and optical properties or biocompatibility which may be enhanced by the modification of Nb_2O_5 films such that they significantly enhance the performance of a device. In the following sections, some of the most common applications of Nb_2O_5 that have been reported in the literature are presented.

4.1 Solar cells and light emitting diodes

Nb_2O_5 films are promising candidates for developing different types of optical devices, including solar cells based on dye-sensitized and heterojunction architectures as well as light emitting diodes (LEDs).
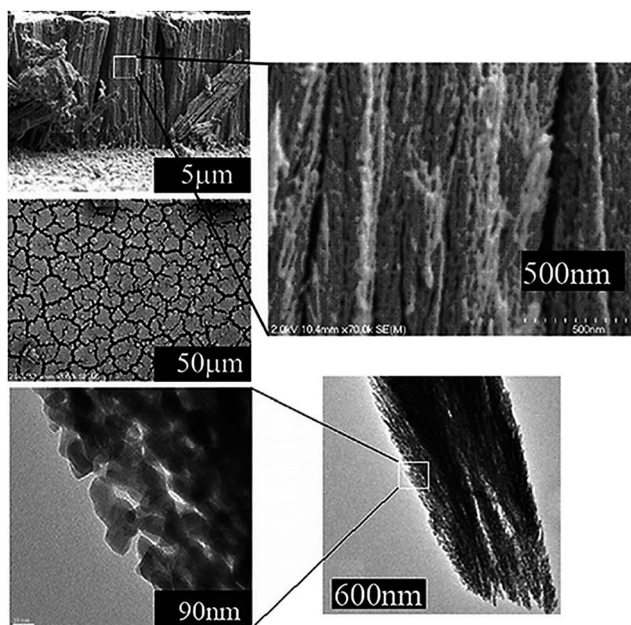

Fig. 8 Top and cross-sectional views (SEM and TEM images) of Nb_2O_5 films deposited using PLD process. Reprinted with permission from ref. 20. Copyright 2011, American Chemical Society.

Since their discovery by Grätzel in 1991, dye sensitized solar cells (DSSCs) have been extensively studied as they offer the potential for clean, reliable, cost effective and on-site energy generation.[185] Increasing the efficiency of DSSCs depends on improving every single element in their structure, including: photoanode, dye, electrolyte and counter-electrode. However, the development of the most suitable photoanode will still have the most significant impact on the DSSCs's performance.[185] Nb_2O_5 has recently drawn considerable attention as a promising photoanode in view of its wider band gap (due to its higher conduction band edge) as well as comparable electron injection efficiency and better chemical stability in comparison to titanium oxide (TiO_2).[23,41,186] These properties of Nb_2O_5 can potentially enhance the DSSCs' efficiency by increasing the open circuit voltage (V_{oc}) and photoconversion efficiency (η).[187]

Several studies have been reported on the synthesis of Nb_2O_5 photoanodes which were obtained using hydrothermal, chemical anodization, sol–gel coating and PLD techniques.[17,20,22,23,38,110,167,188–190] The details are summarized in Table 3. To date, the highest conversion efficiencies of more than 6% have been exhibited by devices with a hydrothermally grown Nb_2O_5 photoanode with the optimum thickness of ~11 μm.[38] Ou et al. and Rani et al. have established an anodization method to obtain Nb_2O_5 nanovein-network photoanodes with large surface areas and low number of impurity defects for DSSCs.[23,110] The photoanodes with no detectable impurities exhibited longer electron lifetimes, indicating more suitability in preventing charge recombination and possible enhancement of the conversion efficiency (Fig. 9). However, the efficiency of the overall devices incorporating these photoanodes was still relatively low (~3.5 to 4.1 %) which was attributed to the lack of the optimisation of the thickness of the Nb_2O_5 frameworks.

Additionally, several researchers have applied Nb_2O_5 films as a blocking layer in DSSCs. Thin Nb_2O_5 films fabricated by spray pyrolysis, sputtering, sol–gel and dip coating methods have been used as potential blocking layers between the contact electrode and the TiO_2 layer, improving the V_{oc} which created a better conversion efficiency for TiO_2 based DSSCs.[176,191–194] Furthermore, it has been shown that a Nb_2O_5 film could play an essential role in increasing the efficiency of the DSSCs as a layer between the TiO_2 photoanode and electrolyte.[195–197] This

Table 3 Summary of DSSCs based on Nb_2O_5 nanostructured films featuring their typical performance data

Photoanode	Efficiency (%)	V_{oc} (V)	J_{sc} (mA cm^{-2})	Thickness/substrate	Refs
Nb_2O_5 with nanochannel structures (anodization process – Nb foil as a substrate)	4.48	0.639	17.6	10.0 μm/Nb foil	22
Nb_2O_5 with nano-vein networks	3.45	0.635	8.72	5.0 μm/FTO glass	110
Nb_2O_5 with nanochannel structures (anodization process – RF sputtered Nb metal on FTO as a substrate)	2.20	0.670	6.91		
Nb_2O_5 with micro-mountain and nano-forest pancake structures (anodization process)	3.35	0.59	10.66	27.7 μm/Nb disk	190
Nb_2O_5 nanorod film (by transforming $Nb_3O_7(OH)$ hydrothermal into Nb_2O_5 nanorods after annealing)	6.03	0.749	12.20	11.2 μm/FTO glass	38
Nb_2O_5 nanoparticle	4.68	0.662	11.57	12.1 μm/FTO glass	
Nb_2O_5 with nano-vein networks (anodization process – Nb foil as substrate)	4.1	0.701	10.00	4.0 μm/Nb foil	23
Nb_2O_5 nanoforest by PLD	2.41	0.710	6.65	5.9 μm/FTO glass	20
Nb_2O_5 thin film deposited by spray pyrolysis	0.98	0.455	1.6	ITO glass	19
Nb_2O_5 nanobelts (powder-air thermal)	1.42	0.580	3.93	10.0 μm/FTO glass	167
Nb_2O_5 sol–gel film with polymeric ligand and carbon soot deposited by spin coating	4.00	0.665	12.20	15.5 μm/FTO glass	17
Nb_2O_5 colloids and adding hydroxypropyl cellulose (hydrolysis and spin coating – autoclave technique)	4.00	0.595	9.70	15.5 μm/FTO glass	202
Nb_2O_5 sol–gel film deposited by spin coating	2.20	0.610	7.00	6.0 μm/FTO glass	121
Nb_2O_5 nanoporous film (powder-air thermal)	2.00	0.630	4.90	8.0 μm/FTO glass	188
Nb_2O_5 ordered needles film (colloidal suspensions were made from hydrolyzed niobate solutions by an autoclave method)	—	0.400	0.53	6.0 μm/ITO glass	189

This journal is © The Royal Society of Chemistry 2014
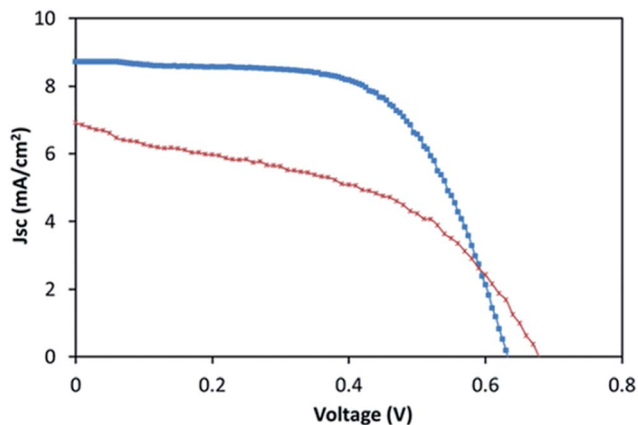
J. Mater. Chem. A, 2014, 2, 15683–15703 | 15693

Fig. 9 Current–voltage (*J–V*) characteristics of DSSCs fabricated using Nb_2O_5 without impurity defects (blue line) and Nb_2O_5 with impurity defects (red line) in the photoanodes. Reprinted with permission from ref. 110. Copyright 2013, Royal Society of Chemistry.

increase was attributed to the coating which either prevented the recombination of electrons and holes due to the barrier effect or the change in the energy level of the TiO_2 conduction band.[197] However, other investigations have disregarded those factors and claimed that the improvement in the performance of the cell could be attributed to an enhancement in the charge injection efficiency promoted by Nb_2O_5.[195] Nb_2O_5 has also been incorporated as a counter electrode in DSSCs. Wu *et al.* and Lin *et al.* have reported a significant conversion efficiency between 4.65 to 5.82% in DSSCs using a Nb_2O_5 counter electrode with a TiO_2 photoanode.[198,199] In these studies, the types of gases used during the annealing treatment and changes in crystallinity of the Nb_2O_5 counter electrode were reported as a factor that influenced the DSSCs' efficiency.

For polymer based bulk heterojunction solar cells, Nb_2O_5 thin films commonly act as electron transport layers.[200,201] It has been found that Nb_2O_5 films are compatible with and have good adhesion properties to many polymer layers.[200]

Wiranwetchayan *et al.* reported that very thin Nb_2O_5 films between the electron collecting electrodes and active layers were necessary to promote the formation of continuous uniform active layers and thus blocking the holes in those layers from being recombined with the electrons in the collecting electrode.[201] However, further investigations of such polymeric solar cells should be considered in order to obtain higher conversion efficiencies.

The capability of Nb_2O_5 films have also been studied in LED applications.[203,204] Su *et al.* applied Nb_2O_5 and SiO_2 films as high and low refractive indices of omnidirectional high reflector (ODR) in white LEDs, respectively.[204] The Nb_2O_5 and SiO_2 pair was chosen due to their high transparencies in the visible and UV wavelength ranges.[71,204] They observed that the leaked UV light escaping from the white LED is completely blocked and remarkably enhanced visible light extraction (400–750 nm) of the white LED which incorporated ODR packaging was enhanced with an average enhancement of 15% in luminous intensity.

4.2 Sensing devices

Like other metal oxides such as TiO_2 and zinc oxide (ZnO), Nb_2O_5 has shown great potential to be used as a sensing material. Sensor devices based on Nb_2O_5 for gas, humidity, biological and chemical sensing as well as photodetection have been successfully demonstrated. Generally, the main parameters for good sensing device performance are the size, morphology, aspect ratio, intergranular connectivity, porosity, surface energy, stoichiometry and surface area to volume ratio of the incorporated sensing material.[205,206]

In 1983, Kondo *et al.* reported the first Nb_2O_5 gas sensors for O_2.[207] Before the nanostructured form of Nb_2O_5 had been introduced in a gas sensor, generally techniques such as RF magnetron sputtering was used to deposit dense Nb_2O_5 films.[15,208–210] Several studies applied metal catalysts such as platinum (Pt) and palladium (Pd) onto the surface of Nb_2O_5, which could promote chemical reactions between the target gas and the oxide film and consequently, increase the sensing capability.[55,211,212] The types of sensing methods or principles that have so far been reported were mainly based on conductometric, voltammetric, chronoamperometric and Schottky contact sensors[15,55,208,209,211–220] Depending on the type of gas species, reducing or oxidizing, the interaction between the gas molecules and the Nb_2O_5 films changes the charge carrier concentration and the potential barrier of the Nb_2O_5 films. These affect the physico-chemical property of the films
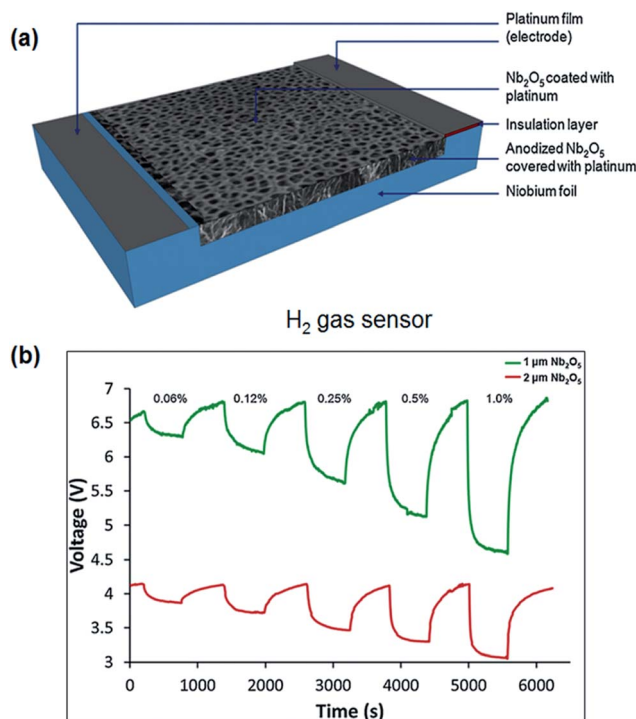

Fig. 10 (a) The schematic of a Schottky based gas sensor made of nanoporous Nb_2O_5 coated with Pt and (b) dynamic response of such Nb_2O_5 gas sensors with 1 and 2 µm thick layers measured with different concentrations of H_2 gas at 100 °C at a constant bias current of 100 µA. Reprinted with permission from ref. 211. Copyright 2013, Elsevier.

15694 | *J. Mater. Chem. A*, 2014, **2**, 15683–15703

This journal is © The Royal Society of Chemistry 2014

corresponding to the gas constituents exposed to the sensor. So far, the investigated gases that have been examined using Nb_2O_5 are O_2, hydrogen (H_2), dissolved O_2, carbon monoxide (CO), ammonia (NH_3) and a number of hydrocarbons (HCs).[15,55,208,209,211–220] An example of a H_2 Schottky based gas sensor based on a Nb_2O_5/Pt contact and the dynamic responses of this device is presented in Fig. 10. For humidity sensing, pellet type Nb_2O_5 sensors have been explored by Yadav et al.[221] More recently, Fiz et al. have synthesized single-crystalline Nb_2O_5 nanorods and SnO_2/Nb_2O_5 core–shell heterostructures by CVD method.[163] The results have demonstrated that the growth of the nanoscopic Nb_2O_5 overlayer on SnO_2 nanowires introduced defects in the structure, which influenced the electronic properties of the material and enabled the design of more efficient sensor.

Due to the chemical stability and corrosion resistance of Nb_2O_5, the material has also been explored for pH and ascorbic acid measurements.[5,222] Furthermore, Nb_2O_5 has also been used as a working electrode in electrochemical based DNA biosensors.[223,224]

Beside gas, chemical and biological sensing, it has been demonstrated that Nb_2O_5 with its wide band gap and long electron life time, is a good candidate for making fast ultraviolet photodetection systems.[225] Fang et al. have shown that a photodetector based on individual Nb_2O_5 nanobelts resulted in a high external quantum-efficiency (EQE) of >6000%.[226]

4.3 Batteries and supercapacitors

The development of energy storage devices based on lithium-ion batteries (LIBs) and supercapacitors have created great interest among researchers and Nb_2O_5 is certainly a favorable material for creating such storage devices.[227–230] Developing devices that can store sustainable energy with long term stability, very prolonged cycle life and meeting environmental constraints as well as safe operating potential windows (in the range of $1.0 \leq V \leq 3.0$ V vs. Li^+/Li) are the main goals of this field.

The study of Nb_2O_5 as an electrode material for lithium ion cells started in the early 1980s.[231,232] The observations by Reichman et al. demonstrated that Nb_2O_5 can undergo intercalation with Li^+, leading to the possibility of repeated charging and discharging.[231] Subsequently, a LIB based on a Nb_2O_5 cathode was studied extensively by the Kumagai group.[183,232–239] The structural changes of the Nb_2O_5 cathodes which are caused by discharging and recharging were investigated using X-ray photoelectron spectroscopy (XPS), X-ray diffraction (XRD) and X-ray absorption fine structure (XAFS) analysis methods.[183,232] They suggested that tetragonal-Nb_2O_5 exhibited the best cycling performance with a large discharge capacity of 190 mA h g^{-1} for up to 30 cycles. XRD analysis suggested that the orthorhombic- and tetragonal-Nb_2O_5 maintain their original crystal lattices, accompanying a small change in the cell volume even after Li^+ intercalation. However, the two-dimensional layered structure of tetragonal-Nb_2O_5 was suggested to be the best for accommodating a large concentration of the intercalating ions.[183] Investigations of Nb_2O_5 LIBs using several electrolytes and

different amounts of graphite in the electrodes have also been reported.[239] It was observed that the discharge capacity decreased with a decrease in the graphite content, and declined to 20–120 mA h per gram oxide in the graphite content range 0–10 wt%. Furthermore, there are also reports on the application of sputtered Nb_2O_5 as a LIB electrode (Fig. 11a and b).[236,238] Nakazawa et al. reported a battery with a sputtered Nb_2O_5 negative electrode of 100 nm thickness showed the most favourable charge–discharge properties with a capacity of 310–380 mA h cm^{-3} for 500 cycles.[238]

Obviously the incorporation of nanostructured Nb_2O_5 should enhance the performance of LIBs. Nb_2O_5 nanobelts were the first nanostructured Nb_2O_5 to be used as an electrode material in LIBs which reported a potential window of 3.0–1.2 V (vs. Li^+/Li).[240] LIBs made of Nb_2O_5 nanobelts demonstrated a high reversible charge–discharge capacity, high rate capability with excellent cycling stability as large as 180 mA h g^{-1} after 50 cycles which could work smoothly even at a high current density of 10 Ag^{-1}. Le Viet et al. reported LIBs based on three different polymorphs of Nb_2O_5 nanofibers prepared by an electro-spinning method and annealing treatment.[31] Among pseudo-hexagonal-, orthorhombic- and monoclinic-Nb_2O_5 nanofibers, the monoclinic based LIB showed the highest capacity, lowest capacity fading and good cycling stability. In addition, Li et al. demonstrated that Nb_2O_5 nanocrystals coated with a thin layer of a homogeneous carbon shell as an electrode demonstrated a relatively long cycle life (130 mA h g^{-1} after over 300 cycles) by preventing the Nb_2O_5 volume change and pulverization during the charge–discharge process.[87] A study on Ta-substituted Nb_2O_5 nanofibers and Nb_2O_5 nanocomposites with various vanadium oxide contents – based LIBs have also been discussed elsewhere.[119,241] A report on a battery based on a Nb_2O_5 anode with a KS-6 graphite cathode showed it to be an inherently safe energy storage system due to no oxygen release from the cathode materials, no lithium dendrite formation and no possibility of overcharge from the electrode/electrolyte reaction.[242] However, the cell capacity and cycling stability of such devices are still considered to be low.

Sasidharan et al. demonstrated a LIB based on Nb_2O_5 hollow nanospheres which can deliver a high capacity of 172 mA h g^{-1} after 250 cycles of charge–discharge that maintained electrode structural integrity with an excellent cycling stability even after exposing it to a high current density of 6.25 Ag^{-1}.[24] In this work, the enhanced LIB's performance was attributed to the hollow cavity coupled with the nanosized Nb_2O_5 shell domain that facilitated fast lithium intercalation/deintercalation kinetics. Meanwhile, anodic Nb_2O_5 electrodes for LIB applications have been reported by Yoo et al.[102] The discharge capacity of 53 µA h cm^{-2} was obtained at 800 nm thick Nb_2O_5 without a surface dissolution layer at a potential window of 1.2–3.0 V. Experiments were also conducted by Rahman et al. using LIB electrodes based on vein-like nanoporous networks of anodic Nb_2O_5 mixed with acetylene carbon black.[103] The device exhibited a reversible capacity of 175 mA h g^{-1} even after 300 cycles at a current density of 0.4 Ag^{-1} and a potential window of 1.2–3.0 V (Fig. 11c and d). This work also demonstrated an excellent reversible discharge capacity at a high current density of 2.6 Ag^{-1}.
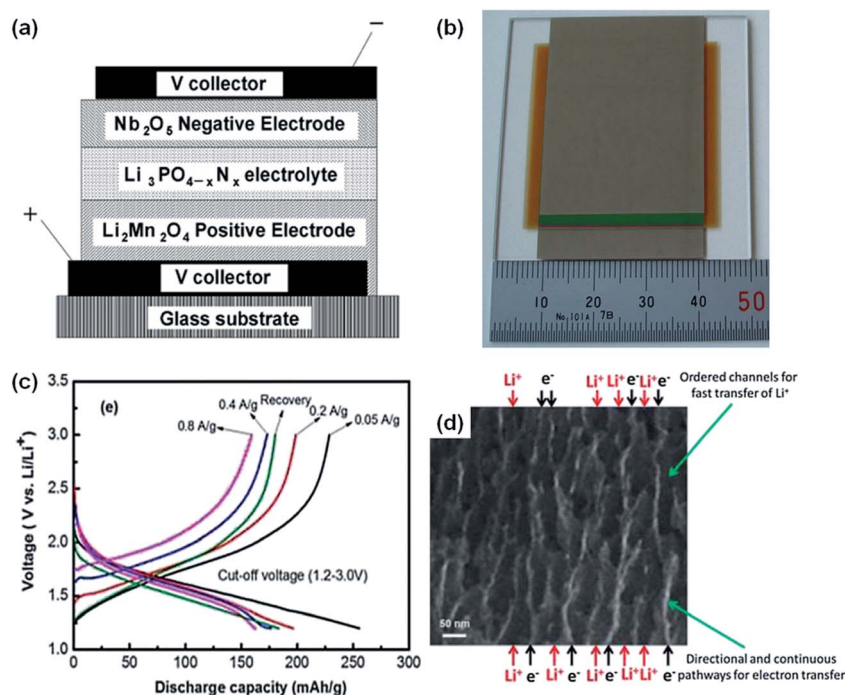
This journal is © The Royal Society of Chemistry 2014

J. Mater. Chem. A, 2014, 2, 15683–15703 | 15695

Fig. 11 (a) A schematic diagram of a thin-filmed $Nb_2O_5/Li_2Mn_2O_4$ battery in a cross-section, and (b) a photograph of a thin-film battery with a 50 mm × 50 mm size in a plane view. (c) Electrochemical performance of the nanoporous Nb_2O_5 electrodes: corresponding galvanostatic discharge–charge voltage profiles for the 1st cycle at each rate. (d) The porous network of Nb_2O_5 with possible fast pathways for Li ions and electrons. (a and b) Reprinted with permission from ref. 238. Copyright 2007, Elsevier, (c and d) reprinted with permission from ref. 103. Copyright 2013, The Royal Society of Chemistry.

In comparison to batteries, supercapacitors (SCs) offer significantly higher power densities with longer cycling life and fast charging. However, the main shortcoming of SCs is their low energy density, due to the restricted storage capacity as a result of the limitation of the size of the electrodes. One possible strategy to address these challenges is to develop high energy density electrodes. The effect of Nb_2O_5 crystallinity on the capacitive response of SCs has been reported by Kim et al.[243] Augustyn et al. have shown that thick electrodes of up to 40 μm offer the promise of exploiting intercalation pseudocapacitance to obtain high-rate charge-storage devices.[244] Another study on understanding the origin of high-rate intercalation pseudocapacitance in Nb_2O_5 crystals was presented by Lubimtsev et al.[245]

So far, incorporation of carbon with Nb_2O_5 to fabricate a composite SC electrode has been considered as one of the most effective solutions in developing high energy density electrodes.[246] Wang et al. developed a SC electrode that consisted of CNT networks intimately mixed with Nb_2O_5 nanocrystals to generate a SC with a high capacitance, excellent rate capability as well as cycling capability.[247] The intimate contact between the nanocrystals and the CNTs enabled fast electron transport and increased current, while the small dimensions of the nanocrystals shortened the lithium-ion diffusion length.

4.4 Catalysts

Nb_2O_5 in its pure form has been used as a high temperature catalyst for the oxidative dehydrogenation (ODH) of organic

materials in their gaseous form such as methane to formaldehyde and propane to propene.[28,248] In addition, other reports have demonstrated that Nb_2O_5 could serve as an efficient catalyst for the transesterification of β-keto esters with several kinds of alcohols, leading to good conversion at acceptable yields.[249] It has been suggested that the catalytic performance of each polymorphic form of Nb_2O_5 differs significantly from one another. However, Nb_2O_5 has commonly been used with other metal oxides/metals due to the following properties that it offers to the composite catalyst:[250–252] (i) promotion and support properties: Nb_2O_5 enhances catalytic activity, selectivity and prolongs catalyst life when a small amount of this oxide is added to known catalysts, (ii) acidic property: the surface acid strength of hydrated Nb_2O_5 exhibits high catalytic activity, selectivity and stability for acid catalysed reactions in which water molecules participate, and (iii) redox properties and photosensitivity: Nb_2O_5 in mixed oxides is an oxidant and demonstrates photosensitivity.

Similar to its pure form, Nb_2O_5 has also been used together with other metal/metal oxide for the dehydrogenation of organic compounds in their gaseous forms.[250,251,253–255] Cherian et al. investigated a Nb_2O_5 supported chromium oxide (Cr_2O_3) catalyst for the ODH of propane to propene which demonstrated more than 80% selectivity in a temperature range of 673–723 K.[254] They also claimed the Nb_2O_5 support did not degrade the propene as much as Al_2O_3 and TiO_2 supports. The ODH of propane was also investigated by the addition of 1 to 20 wt % of Nb_2O_5 in Pd/Al_2O_3 catalysts (Fig. 12).[256] Similar catalytic properties have also been

15696 | J. Mater. Chem. A, 2014, **2**, 15683–15703

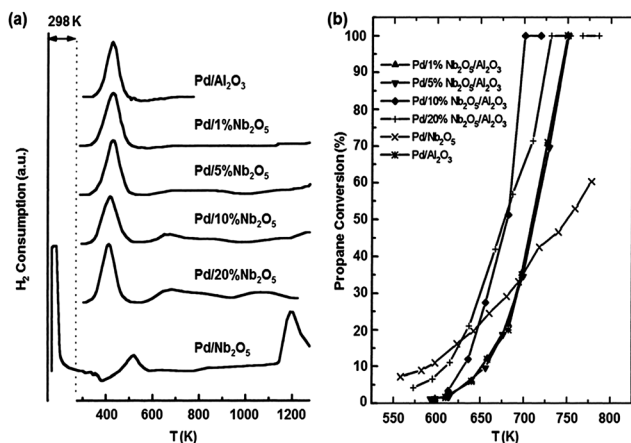This journal is © The Royal Society of Chemistry 2014

Fig. 12 (a) Temperature-programmed reduction (TPR) profile of Pd/Nb$_2$O$_5$/Al$_2$O$_3$ catalysts. (b) Conversion of propane as a function of the reaction temperature for Pd/Nb$_2$O$_5$/Al$_2$O$_3$ catalysts at different ratios. Reprinted with permission from ref. 256. Copyright 2000, Elsevier.

Fig. 13 SEM images of anodized Nb$_2$O$_5$ films and the coloration efficiency of 500 nm, 750 nm, and 1 μm thick anodized Nb$_2$O$_5$ films under chronoamperometric (CA) at ±1.5 V applied potential for the optical wavelength of 550 nm. Reprinted with permission from ref. 69. Copyright 2014, American Chemical Society.

shown for other metal oxide compounds with Nb$_2$O$_5$ including Re$_2$O$_7$, CrO$_3$, WO$_3$, MoO$_3$, and V$_2$O$_5$.[257]

Nb$_2$O$_5$ has also been utilised as a photocatalyst. Under illumination, Nb$_2$O$_5$ produces electron/hole pairs that can generate hydroxyl radicals ($^\bullet$HO) from water, which are able to undergo further reactions in solution. Such photocatalytic applications have been successfully demonstrated for water splitting and degradation of harmful organic contaminants.[47,89,258–263] Increased photocatalytic activity was achieved by forming Nb$_2$O$_5$ nanostructures such as mesoporous, electrospun nanofibers, nanorods and nanospheres as a result of their high surface area.[258,262] The addition of metal particles (i.e., Pt, Au, Cu) and metal oxides (i.e., CuO, NiO) into a Nb$_2$O$_5$ photocatalysts can delay the electron and hole recombination rate which enhances reduction reactions and improves the hydrogen production rate.[259,260] Furthermore, carbon incorporation is also an effective technique to enhance photocatalytic activity. This is due to the capability of the carbon to modify the surface chemical composition of Nb$_2$O$_5$ and extend its absorption into the visible light range.[262]

4.5 Electrochromic devices

Electrochromism is the ability of a material to change its transparency upon exposure to stimuli. Electrochromic (EC) materials are at the core of a variety of applications including smart windows for architectural and automotive industries as well as optical displays.[264–266] An ideal EC material should have high initial transparency, large optical contrast between coloured and bleach states, short switching time, and long-term cyclic stability.[267]

Nb$_2$O$_5$ has an excellent potential for the development of EC systems. It has multicolour capabilities and it also shows long-term cyclic stability due to its relatively large band gap.[268,269] To date, the best EC ever reported has been for elevated temperature anodized Nb$_2$O$_5$ showing values as large as 47.0 cm^2 C^{-1} at an applied potential of −1.5 V for samples of 500 nm thickness (Fig. 13).[69] Other studies of EC systems based on Nb$_2$O$_5$ films using
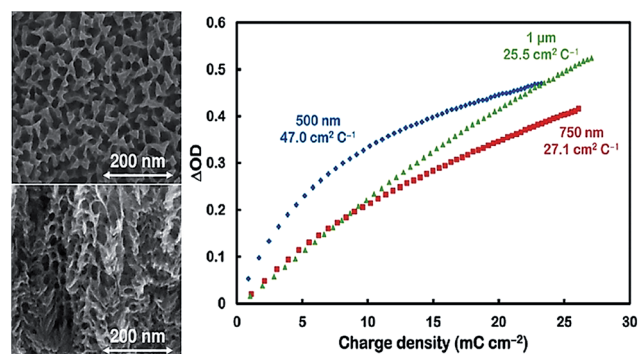
other synthesis techniques including sol–gel, thermal oxidation, chemical vapour deposition and pulse-laser deposition have also been reported elsewhere but resulted in lower ECs.[16,29,67,118,153,269–272]

4.6 Other applications

Nb$_2$O$_5$ has also been reported for applications other than those presented in Sections 4.1 to 4.5. As highlights, Nb$_2$O$_5$ has been incorporated in electronic devices such as memristors, capacitors, and field-effect transistors (FETs).

Highly crystalline orthorhombic Nb$_2$O$_5$ nanofibers obtained by electrospinning have been used in the development of memristors.[273] Reproducible bipolar resistive switching with an ON–OFF resistance ratio as high as 2 × 10^4 was observed in individual fibers. Hota et al. investigated the performance of Pd nano-dots (NDs) embedded in Nb$_2$O$_5$ memristors by scanning tunnelling microscopy.[30] From the current–voltage measurements, the memristors showed non-volatile memory and bipolar resistive switching characteristics. They claimed that the inclusion of Pd NDs played a critical role by acting as oxygen ion reservoirs and/or by polarizing a large volume of oxygen vacancies.[30] In addition, non-volatile resistive switching behaviour was also demonstrated at anodic Nb$_2$O$_5$ based memristors (in the configuration of Au/Nb$_2$O$_5$/Nb/Si sandwich memory cells).[274] The devices exhibited reproducible performance with a resistance ON–OFF ratio of ~10^3.

Meanwhile, an interesting report on a capacitor based on Nb$_2$O$_5$ was presented by Garcia et al., who investigated the influence of the growth and annealing temperatures on the electrical properties of Nb$_2$O$_5$ based MIM capacitors.[64] The obtained results show that the permittivity values exceeded 50 for the films crystallized after annealing at temperatures higher than 500 °C. However, the leakage current values for the crystalline films were higher than those in the case of amorphous films.

It has also been shown recently that Nb$_2$O$_5$ can be used in FETs by Kao et. al.[275] The gain of the device could be readily controlled via the gate voltage modulations. The same group also showed the incorporation of such a FET as transducers for pH and biosensing.

5. Conclusion and future outlook

In this comprehensive review, we have presented the fundamental physical and chemical properties of Nb_2O_5, focusing on crystal structure and its electrical, optical, mechanical and thermal properties. In addition, we also discussed the various techniques that have been used to synthesize various forms of Nb_2O_5, and the most commonly reported applications incorporating Nb_2O_5 were summarized.

It was highlighted that Nb_2O_5 is found in a variety of crystal phases. The most common phases that are observed include pseudohexagonal, orthorhombic and monoclinic. There are still many unsubstantiated statements regarding the crystal structures of Nb_2O_5, especially when sub stoichiometry is present, thus more rigorous crystal phase analysis should be conducted to shed light on such conflicting arguments. Tetragonal Nb_2O_5, which is an unstable crystal structure between the orthorhombic and monoclinic phases, is still not well understood and less explored, which may present an opportunity for future research.

The reports regarding band energy diagrams, and as a result, the electronic and optical properties of Nb_2O_5 were presented. The mechanical and thermal properties of Nb_2O_5 were also discussed. However, it was hinted that many fundamental topics such as the Seebeck coefficient, thermal conductivity and carrier mobility of Nb_2O_5 have been rarely studied opening great avenues for future investigations.

Numerous synthesis techniques of Nb_2O_5 were briefly discussed in this review. It was seen that there exists a wide range of nanostructured Nb_2O_5 that have been successfully synthesized including nanoporous, nanosheets, nanorods, nanochannels, and nanowires, among others. However, a variety of other Nb_2O_5 morphologies have yet to be explored and fully characterized. We also believe that simple synthesis methods and low cost production routes should be investigated in more detail.

We have described numerous applications of Nb_2O_5 in catalysis, electrochromic devices, batteries, sensors and solar cells. However, many of these studies are still in their infancy and require further exploration. For example, in solar cell applications, Nb_2O_5 has received relatively little attention compared to materials such as TiO_2 and ZnO even though theoretically, Nb_2O_5 in both dye sensitized and heterostructure systems can offer enhanced efficiency. Furthermore, Nb_2O_5 in transistor, memristor and superconductor devices has been less studied compared to other metal oxides. There are certainly significant chances for further investigations of the capabilities of these devices through the exploitation of nanostructured Nb_2O_5.

Since Nb_2O_5 demonstrates excellent mechanical flexibility and durability as well as fantastic electronic and optical properties, one should consider the opportunity for its use in microelectro-mechanical systems (MEMS) and sensors, especially in combination with microfluidics and biomedical devices. There are many more applications that can be considered and comprehensive studies using Nb_2O_5 in many relevant fields should be encouraged, since its capability in many applications has not yet been examined.

Notes and references

1 F. Holtzberg, A. Reisman, M. Berry and M. Berkenblit, *J. Am. Chem. Soc.*, 1957, **79**, 2039–2043.
2 G. Brauer, *Z. Anorg. Allg. Chem.*, 1941, **248**, 1–31.
3 H. Schäfer, R. Gruehn and F. Schulte, *Angew. Chem., Int. Ed. Engl.*, 1966, **5**, 40–52.
4 M. P. F. Graca, A. Meireles, C. Nico and M. A. Valente, *J. Alloys Compd.*, 2013, **553**, 177–182.
5 L. T. Arenas, P. C. M. Villis, J. Arguello, R. Landers, E. V. Benvenutti and Y. Gushikem, *Talanta*, 2010, **83**, 241–248.
6 D. Velten, E. Eisenbarth, N. Schanne and J. Breivie, *J. Mater. Sci.: Mater. Med.*, 2004, **15**, 457–461.
7 R. Pinto and B. M. Shaha, *Jpn. J. Appl. Phys.*, 1968, **7**, 1542.
8 B. Lelevic, N. Fuschillo and N. K. Annamalai, *Thin Solid Films*, 1974, **23**, 249–256.
9 P. Griesmar, G. Papin, C. Sanchez and J. Livage, *Chem. Mater.*, 1991, **3**, 335–339.
10 G. R. Lee and J. A. Crayston, *J. Mater. Chem.*, 1991, **1**, 381–386.
11 N. Machida, M. Tatsumisago and T. Minami, *J. Electrochem. Soc.*, 1986, **133**, 1963–1966.
12 E. I. Ko, J. M. Hupp and N. J. Wagner, *J. Chem. Soc., Chem. Commun.*, 1983, 94–95.
13 K. Kunimori, H. Abe and T. Uchijima, *Chem. Lett.*, 1983, 1619–1622.
14 A. V. Chadwick, W. Zhou and J. M. Thomas, *Angew. Chem., Int. Ed. Engl.*, 1989, **28**, 75–76.
15 D. Rosenfeld, P. E. Schmid, S. Széles, F. Lévy, V. Demarne and A. Grisel, *Sens. Actuators, B*, 1996, **37**, 83–89.
16 M. A. B. Gomes, L. O. d. S. Bulhões, S. C. de Castro and A. J. Damião, *J. Electrochem. Soc.*, 1990, **137**, 3067–3070.
17 M. A. Aegerter, M. Schmitt and Y. P. Guo, *Int. J. Photoenergy*, 2002, **4**, 1–10.
18 Ö. D. Coşkun and S. Demirela, *Appl. Surf. Sci.*, 2013, **277**, 35–39.
19 M. Kovendhan, D. P. Joseph, P. Manimuthu, S. Ganesan, S. Sambasivam, P. Maruthamuthu, S. A. Suthanthiraraj, C. Venkateswaran and R. Mohan, *Trans. Indian Inst. Met.*, 2011, **64**, 185–188.
20 R. Ghosh, M. K. Brennaman, T. Uher, M.-R. Ok, E. T. Samulski, L. E. McNeil, T. J. Meyer and R. Lopez, *ACS Appl. Mater. Interfaces*, 2011, **3**, 3929–3935.
21 C. Nico, L. Rino, M. Matos, R. Monteiro, F. M. Costa, T. Monteiro and M. P. F. Graça, *J. Eur. Ceram. Soc.*, 2013, **33**, 3077–3083.
22 R. Abdul Rani, A. S. Zoolfakar, J. Subbiah, J. Z. Ou and K. Kalantar-Zadeh, *Electrochem. Commun.*, 2014, **40**, 20–23.
23 J. Z. Ou, R. A. Rani, M. H. Ham, M. R. Field, Y. Zhang, H. Zheng, P. Reece, S. Zhuiykov, S. Sriram, M. Bhaskaran, R. B. Kaner and K. Kalantar-Zadeh, *ACS Nano*, 2012, **6**, 4045–4053.
24 M. Sasidharan, N. Gunawardhana, M. Yoshio and K. Nakashima, *Mater. Res. Bull.*, 2012, **47**, 2161–2164.

25 K. Kamada, M. Mukai and Y. Matsumoto, *Electrochim. Acta*, 2004, **49**, 321–327.

26 S. Abe, *Nanoscale Res. Lett.*, 2012, **7**, 1–6.

27 A. Le Viet, R. Jose, M. V. Reddy, B. V. R. Chowdari and S. Ramakrishna, *J. Phys. Chem. C*, 2010, **114**, 21795–21800.

28 B. Michalkiewicz, J. Srenscek-Nazzal, P. Tabero, B. Grzmil and U. Narkiewicz, *Chem. Pap.*, 2008, **62**, 106–113.

29 A. Michel, *Sol. Energy Mater. Sol. Cells*, 2001, **68**, 401–422.

30 M. K. Hota, M. K. Bera, S. Verma and C. K. Maiti, *Thin Solid Films*, 2012, **520**, 6648–6652.

31 A. Le Viet, M. V. Reddy, R. Jose, B. V. R. Chowdari and S. Ramakrishna, *J. Phys. Chem. C*, 2009, **114**, 664–671.

32 I. Nowak and A. M. Ziolek, *Chem. Rev.*, 1999, **99**, 3603–3624.

33 L. A. Reznichenko, V. V. Akhnazarova, L. A. Shilkina, O. N. Razumovskaya and S. I. Dudkina, *Crystallogr. Rep.*, 2009, **54**, 483–491.

34 E. I. Ko and J. G. Weissman, *Catal. Today*, 1990, **8**, 27–36.

35 W. Mertin, S. Andersson and R. Gruehn, *J. Solid State Chem.*, 1970, **1**, 419–424.

36 E. Tsang, X. Zhou, L. Ye and S. C. Edman Tsang, *Nano Rev.*, 2012, **3**, 17631.

37 Y. Kobayashi, H. Hata, M. Salama and T. E. Mallouk, *Nano Lett.*, 2007, **7**, 2142–2145.

38 H. Zhang, Y. Wang, D. Yang, Y. Li, H. Liu, P. Liu, B. J. Wood and H. Zhao, *Adv. Mater.*, 2012, **24**, 1598–1603.

39 J. S. Anderson, J. M. Browne and J. L. Hutchison, *Nature*, 1972, **237**, 151–153.

40 T. Ikeya and M. Senna, *J. Non-Cryst. Solids*, 1988, **105**, 243–250.

41 H. Luo, W. Song, P. G. Hoertz, K. Hanson, R. Ghosh, S. Rangan, M. K. Brennaman, J. J. Concepcion, R. A. Binstead, R. A. Bartynski, R. Lopez and T. J. Meyer, *Chem. Mater.*, 2012, **25**, 122–131.

42 J. W. Schultze and M. M. Lohrengel, *Electrochim. Acta*, 2000, **45**, 2499–2513.

43 T. Proslier, J. Zasadzinski, L. Cooley, M. Pellin, J. Norem, J. Elam, C. Z. Antoine, R. A. Rimmer and P. Kneisel, *IEEE Trans. Appl. Supercond.*, 2009, **19**, 1404–1408.

44 S. Zhuiykov and E. Kats, *World Academy of Science, Engineering and Technology*, 2013, vol. 78.

45 A. D. Yoffe, *Adv. Phys.*, 2002, **51**, 799–890.

46 K. Sattler, *The energy gap of clusters, nanoparticles, and quantum dots*, Academic Press, New York, 2002.

47 A. Esteves, L. C. A. Oliveira, T. C. Ramalho, M. Goncalves, A. S. Anastacio and H. W. P. Carvalho, *Catal. Commun.*, 2008, **10**, 330–332.

48 J. Liu, D. Xue and K. Li, *Nanoscale Res. Lett.*, 2011, **6**, 138.

49 R. Brayner and F. Bozon-Verduraz, *Phys. Chem. Chem. Phys.*, 2003, **5**, 1457–1466.

50 G. Agarwal and G. B. Reddy, *J. Mater. Sci.: Mater. Electron.*, 2005, **16**, 21–24.

51 M. Palatnikov, O. Shcherbina, N. Sidorov and K. Bormanis, *Ukr. J. Phys. Opt.*, 2012, **13**, 207.

52 L. K. Frevel and H. W. Rinn, *Anal. Chem.*, 1955, **27**, 1329–1330.

53 O. Kubaschewski and B. E. Hopkins, *J. Less-Common Met.*, 1960, **2**, 172–180.

54 W. T. Holser, *Acta Crystallogr.*, 1956, **9**, 196–196.

55 Z. Wang, Y. Hu, W. Wang, X. Zhang, B. Wang, H. Tian, Y. Wang, J. Guan and H. Gu, *Int. J. Hydrogen Energy*, 2012, **37**, 4526–4532.

56 R. Norin and A. Magnéli, *Naturwissenschaften*, 1960, **47**, 354–355.

57 B. M. Gatehouse and A. D. Wadsley, *Acta Crystallogr.*, 1964, **17**, 1545–1554.

58 K. Kato, *Acta Crystallogr., Sect. B: Struct. Crystallogr. Cryst. Chem.*, 1976, **32**, 764–767.

59 S. Aggarwal and R. Ramesh, *Ann. Rev. Mater. Sci.*, 1998, **28**, 463–499.

60 E. H. Greener, D. H. Whitmore and M. E. Fine, *J. Chem. Phys.*, 1961, **34**, 1017–1023.

61 P. Kofstad, *J. Phys. Chem. Solids*, 1962, **23**, 1571.

62 W. K. Chen and R. A. Swalin, *J. Phys. Chem. Solids*, 1966, **27**, 57–64.

63 S. Clima, G. Pourtois, S. Van Elshocht, S. De Gendt, M. M. Heyns, D. J. Wouters and J. A. Kittl, *ECS Trans.*, 2009, **19**, 729–737.

64 H. García, H. Castán, E. Perez, S. Dueñas, L. Bailón, T. Blanquart, J. Niinistö, K. Kukli, M. Ritala and M. Leskelä, *Semicond. Sci. Technol.*, 2013, **28**, 055005.

65 G. E. Cavigliasso, M. J. Esplandiu and V. A. Macagno, *J. Appl. Electrochem.*, 1998, **28**, 1213–1219.

66 J. Yahia, *J. Phys. Chem. Solids*, 1964, **25**, 881–887.

67 A. Pawlicka, M. Atik and M. A. Aegerter, *Thin Solid Films*, 1997, **301**, 236–241.

68 M. Schmitt, S. Heusing, M. A. Aegerter, A. Pawlicka and C. Avellaneda, *Sol. Energy Mater. Sol. Cells*, 1998, **54**, 9–17.

69 D. D. Yao, R. A. Rani, A. P. O'Mullane, K. Kalantar-Zadeh and J. Z. Ou, *J. Phys. Chem. C*, 2014, **118**, 476–481.

70 E. Çetinörgü-Goldenberg, J.-E. Klemberg-Sapieha and L. Martinu, *Appl. Opt.*, 2012, **51**, 6498–6507.

71 C.-C. Lee, C.-L. Tien and J.-C. Hsu, *Appl. Opt.*, 2002, **41**, 2043–2047.

72 N. Özer, M. D. Rubin and C. M. Lampert, *Sol. Energy Mater. Sol. Cells*, 1996, **40**, 285–296.

73 X. Xiao, G. Dong, C. Xu, H. He, H. Qi, Z. Fan and J. Shao, *Appl. Surf. Sci.*, 2008, **255**, 2192–2195.

74 O. B. Shcherbina, M. N. Palatnikov and V. V. Efremov, *Inorg. Mater.*, 2012, **48**, 433–438.

75 S. Park, G. Wang, B. Cho, Y. Kim, S. Song, Y. Ji, M.-H. Yoon and T. Lee, *Nat. Nano*, 2012, **7**, 438–442.

76 J. Lewis, *Mater. Today*, 2006, **9**, 38–45.

77 J. Hu, L. Li, H. Lin, P. Zhang, W. Zhou and Z. Ma, *Opt. Mater. Express*, 2013, **3**, 1313–1331.

78 C. Peng, Z. Jia, H. Neilson, T. Li and J. Lou, *Adv. Eng. Mater.*, 2013, **15**, 250–256.

79 M. K. Hota, M. K. Bera and C. K. Maiti, *Semicond. Sci. Technol.*, 2012, **27**, 105001.

80 W. R. Manning, O. Hunter, F. W. Calderwood and D. W. Stacy, *J. Am. Ceram. Soc.*, 1972, **55**, 342–347.

81 D. L. Douglass, *J. Less-Common Met.*, 1963, **5**, 151–157.

This journal is © The Royal Society of Chemistry 2014

J. Mater. Chem. A, 2014, **2**, 15683–15703 | **15699**

82 G. L. Dwivedi and E. C. Subbarao, *J. Am. Ceram. Soc.*, 1973, **56**, 443–444.

83 H. Choosuwan, R. Guo, A. S. Bhalla and U. Balachandran, *J. Appl. Phys.*, 2002, **91**, 5051–5054.

84 M. N. Palatnikov, O. B. Shcherbina, A. A. Frolov, V. N. Pavlikov, M. V. Karpets, O. V. Makarova, N. V. Sidorov and V. T. Kalinnikov, *Inorg. Mater.*, 2010, **46**, 683–690.

85 K. E. Jesse, *J. Appl. Phys.*, 1969, **40**, 3386–3389.

86 H. Luo, M. Wei and K. Wei, *Mater. Chem. Phys.*, 2010, **120**, 6–9.

87 G. Li, X. Wang and X. Ma, *J. Energy Chem.*, 2013, **22**, 357–362.

88 O. F. Lopes, E. C. Paris and C. Ribeiro, *Appl. Catal., B*, 2014, **144**, 800–808.

89 Y. Zhao, C. Eley, J. Hu, J. S. Foord, L. Ye, H. He and S. C. E. Tsang, *Angew. Chem., Int. Ed.*, 2012, **51**, 3846–3849.

90 G. K. M. K. Shankar, H. E. Prakasam, S. Yoriya, M. Paulose, O. K. Varghese and C. A. Grimes, *Nanotechnology*, 2007, **18**, 065707.

91 D. Regonini, C. R. Bowen, A. Jaroenworaluck and R. Stevens, *Mater. Sci. Eng., R*, 2013, **74**, 377–406.

92 P. H. G. Draper and J. Harvey, *Acta Metall.*, 1963, **11**, 873–879.

93 G. C. Wood and C. Pearson, *Nature*, 1965, **208**, 547–549.

94 M. R. Arora and R. Kelly, *J. Mater. Sci.*, 1977, **12**, 1673–1684.

95 A. Aladjem, D. G. Brandon, J. Yahalom and J. Zahavi, *Electrochim. Acta*, 1970, **15**, 663–671.

96 H. Habazaki, Y. Oikawa, K. Fushimi, Y. Aoki, K. Shimizu, P. Skeldon and G. E. Thompson, *Electrochim. Acta*, 2009, **54**, 946–951.

97 J. H. L. Jinsub Choi, J. Lee and K. J. Kim, *Nanotechnology*, 2007, **18**, 055603.

98 J. Choi, J. H. Lim, S. C. Lee, J. H. Chang, K. J. Kim and M. A. Cho, *Electrochim. Acta*, 2006, **51**, 5502–5507.

99 Y. Oikawa, T. Minami, H. Mayama, K. Tsujii, K. Fushimi, Y. Aoki, P. Skeldon, G. E. Thompson and H. Habazaki, *Acta Mater.*, 2009, **57**, 3941–3946.

100 Q. Lu, T. Hashimoto, P. Skeldon, G. E. Thompson, H. Habazaki and K. Shimizu, *Electrochem. Solid-State Lett.*, 2005, **8**, B17–B20.

101 I. Sieber, H. Hildebrand, A. Friedrich and P. Schmuki, *Electrochem. Commun.*, 2005, **7**, 97–100.

102 J. E. Yoo, J. Park, G. Cha and J. Choi, *Thin Solid Films*, 2013, **531**, 583–587.

103 M. M. Rahman, R. A. Rani, A. Z. Sadek, A. S. Zoolfakar, M. R. Field, T. Ramireddy, K. Kalantar-zadeh and Y. Chen, *J. Mater. Chem. A*, 2013, **1**, 11019–11025.

104 J. Zhao, X. Wang, R. Xu, Y. Mi and Y. Li, *Electrochem. Solid-State Lett.*, 2007, **10**, C31–C33.

105 R. L. Karlinsey, *Electrochem. Commun.*, 2005, **7**, 1190–1194.

106 R. L. Karlinsey, *J. Mater. Sci.*, 2006, **41**, 5017–5020.

107 S. Yang, Y. Aoki and H. Habazaki, *Appl. Surf. Sci.*, 2011, **257**, 8190–8195.

108 W. Wei, K. Lee, S. Shaw and P. Schmuki, *Chem. Commun.*, 2012, **48**, 4244–4246.

109 K. Lee, Y. Yang, M. Yang and P. Schmuki, *Chem.–Eur. J.*, 2012, **18**, 9521–9524.

110 R. A. Rani, A. S. Zoolfakar, J. Z. Ou, R. Ab Kadir, H. Nili, K. Latham, S. Sriram, M. Bhaskaran, S. Zhuiykov, R. B. Kaner and K. Kalantar-Zadeh, *Chem. Commun.*, 2013, **49**, 6349–6351.

111 S. Barredo-Damas, K. Lee, R. Kirchgeorg, R. Sánchez-Tovar and P. Schmuki, *ECS Electrochem. Lett.*, 2013, **2**, C4–C6.

112 L. L. Hench and J. K. West, *Chem. Rev.*, 1990, **90**, 33–72.

113 M. Niederberger and N. Pinna, in *Metal Oxide Nanoparticles in Organic Solvents*, Springer, London, 2009, ch. 2, pp. 7–18.

114 A. Pierre, in *Introduction to Sol-Gel Processing*, Springer, USA, 1998, vol. 1, ch. 1, pp. 1–9.

115 T. Olding, M. Sayer and D. Barrow, *Thin Solid Films*, 2001, **398**, 581–586.

116 C. Alquier, M. T. Vandenborre and M. Henry, *J. Non-Cryst. Solids*, 1986, **79**, 383–395.

117 N. Ozer, T. Barreto, T. Buyuklimanli and C. M. Lampert, *Sol. Energy Mater. Sol. Cells*, 1995, **36**, 433–443.

118 P. R. Bueno, C. O. Avellaneda, R. C. Faria and L. O. S. Bulhoes, *Electrochim. Acta*, 2001, **46**, 2113–2118.

119 G. Li, X. Wang, Z. Chen, X. Ma and Y. Lu, *Electrochim. Acta*, 2013, **102**, 351–357.

120 L. Melo, C. O. Avellaneda and A. Pawlicka, *Mol. Cryst. Liq. Cryst.*, 2002, **374**, 101–106.

121 P. Guo and M. A. Aegerter, *Thin Solid Films*, 1999, **351**, 290–294.

122 M. Ristic, S. Popovic and S. Music, *Mater. Lett.*, 2004, **58**, 2658–2663.

123 D. A. de Barros Filho, P. P. Abreu Filho, U. Werner and M. A. Aegerter, *J. Sol-Gel Sci. Technol.*, 1997, **8**, 735–742.

124 T. Sreethawong, S. Ngamsinlapasathian and S. Yoshikawa, *Mater. Lett.*, 2012, **78**, 135–138.

125 M. H. Habibi and R. Mokhtari, *J. Inorg. Organomet. Polym. Mater.*, 2012, **22**, 158–165.

126 I. Zhitomirsky, *J. Eur. Ceram. Soc.*, 1999, **19**, 2581–2587.

127 I. Zhitomirsky, *Mater. Lett.*, 1998, **35**, 188–193.

128 J.-H. Jang, T.-Y. Kim, N.-J. Kim, C.-H. Lee, E.-M. Park, C. Park and S.-J. Suh, *Mater. Sci. Eng., B*, 2011, **176**, 1505–1508.

129 D. Yang, *Nanocomposite films for gas sensing, advances in nanocomposites - Synthesis, characterization and industrial applications*, InTech, 2011.

130 Y. K. Yap, *Physical Vapor Deposition, Encyclopedia of Nanotechnology: Springer Reference*, Springer, Berlin Heidelberg, 2012.

131 F. Richter, H. Kupfer, P. Schlott, T. Gessner and C. Kaufmann, *Thin Solid Films*, 2001, **389**, 278–283.

132 B. Hunsche, M. Vergöhl, H. Neuhäuser, F. Klose, B. Szyszka and T. Matthée, *Thin Solid Films*, 2001, **392**, 184–190.

133 S. Venkataraj, R. Drese, O. Kappertz, R. Jayavel and M. Wuttig, *Phys. Status Solidi A*, 2001, **188**, 1047–1058.

134 K. Yoshimura, T. Miki and S. Tanemura, *J. Electrochem. Soc.*, 1997, **144**, 2982–2985.

135 H. Mähne, L. Berger, D. Martin, V. Klemm, S. Slesazeck, S. Jakschik, D. Rafaja and T. Mikolajick, *Solid-State Electron.*, 2012, **72**, 73–77.

136 J. M. Chappé, P. Carvalho, S. Lanceros-Mendez, M. I. Vasilevskiy, F. Vaz, A. V. Machado, M. Fenker, H. Kappl, N. M. G. Parreira, A. Cavaleiro and E. Alves, *Surf. Coat. Technol.*, 2008, **202**, 2363–2367.

137 A. Dhar and T. L. Alford, *J. Appl. Phys.*, 2012, **112**, 103113.

138 F. Lai, M. Li, H. Wang, H. Hu, X. Wang, J. G. Hou, Y. Song and Y. Jiang, *Thin Solid Films*, 2005, **488**, 314–320.

139 F. Lai, L. Lin, Z. Huang, R. Gai and Y. Qu, *Appl. Surf. Sci.*, 2006, **253**, 1801–1805.

140 A. Pignolet, G. M. Rao and S. B. Krupanidhi, *Thin Solid Films*, 1995, **261**, 18–24.

141 R. C. Lee and C. R. Aita, *J. Appl. Phys.*, 1991, **70**, 2094–2103.

142 S. V. Zaitsev, Y. V. Gerasimenko, S. N. Saltykov, D. A. Khoviv and A. M. Khoviv, *Inorg. Mater.*, 2011, **47**, 412–416.

143 T. Maruyama and S. Arai, *Appl. Phys. Lett.*, 1993, **63**, 869–870.

144 L. Berger, H. Maehne, V. Klemm, A. Leuteritz, T. Mikolajick and D. Rafaja, *Appl. Phys. A: Mater. Sci. Process.*, 2012, **108**, 431–437.

145 Y. Shao, K. Yi, M. Fang and J. Zhang, in *Pacific Rim Laser Damage 2011: Optical Materials for High Power Lasers*, ed. J. Shao, K. Sugioka and C. J. Stolz, 2012, vol. 8206.

146 G. Ramírez, S. E. Rodil, S. Muhl, D. Turcio-Ortega, J. J. Olaya, M. Rivera, E. Camps and L. Escobar-Alarcón, *J. Non-Cryst. Solids*, 2010, **356**, 2714–2721.

147 H. Wender, P. Migowski, A. F. Feil, S. R. Teixeira and J. Dupont, *Coord. Chem. Rev.*, 2013, **257**, 2468–2483.

148 P. J. Kelly and R. D. Arnell, *Vacuum*, 2000, **56**, 159–172.

149 C.-L. Tien, *Appl. Surf. Sci.*, 2010, **257**, 481–486.

150 C. M. Cotell, S. Schiestel, C. A. Carosella, S. Flom, G. K. Hubler and D. L. Knies, *Nucl. Instrum. Methods Phys. Res., Sect. B*, 1997, **127–128**, 557–561.

151 B. Reichman and A. J. Bard, *J. Electrochem. Soc.*, 1980, **127**, 241–242.

152 M. Vinnichenko, A. Rogozin, D. Grambole, F. Munnik, A. Kolitsch, W. Möller, O. Stenzel, S. Wilbrandt, A. Chuvilin and U. Kaiser, *Appl. Phys. Lett.*, 2009, **95**, 081904.

153 Z. W. Fu, J. J. Kong and Q. Z. Qin, *J. Electrochem. Soc.*, 1999, **146**, 3914–3918.

154 S. Hyunjun, C. Dooho, L. Dongsoo, S. Seo, L. Myong-Jae, Y. In-Kyeong and H. Hyunsang, *IEEE Electron Device Lett.*, 2005, **26**, 292–294.

155 M. E. Gimon-Kinsel and K. J. Balkus Jr, *Microporous Mesoporous Mater.*, 1999, **28**, 113–123.

156 K. L. Choy, *Prog. Mater. Sci.*, 2003, **48**, 57–170.

157 Y. Kuzminykh, A. Dabirian, M. Reinke and P. Hoffmann, *Surf. Coat. Technol.*, 2013, **230**, 13–21.

158 C. B. da Silveira, A. F. de Oliveira, S. D. de Campos, E. A. de Campos and A. D. Fraporti, *Surf. Eng.*, 2012, **28**, 68–72.

159 N. Hara, E. Takahashi, J. H. Yoon and K. Sugimoto, *J. Electrochem. Soc.*, 1994, **141**, 1669–1674.

160 J. P. Masse, H. Szymanowski, O. Zabeida, A. Amassian, J. E. Klemberg-Sapieha and L. Martinu, *Thin Solid Films*, 2006, **515**, 1674–1682.

161 S. A. O'Neill, I. P. Parkin, R. J. H. Clark, A. Mills and N. Elliott, *J. Mater. Chem.*, 2003, **13**, 2952–2956.

162 A. F. de Oliveira, C. B. da Silveira, S. D. de Campos, E. A. de Campos and E. Carasek, *Talanta*, 2005, **66**, 74–79.

163 R. Fiz, F. Hernandez-Ramirez, T. Fischer, L. Lopez-Conesa, S. Estrade, F. Peiro and S. Mathur, *J. Phys. Chem. C*, 2013, **117**, 10086–10094.

164 W. Hu, Z. Liu, D. Tian, S. Zhang, Y. Zhao and K. Yao, *J. Wuhan Univ. Technol., Mater. Sci. Ed.*, 2009, **24**, 245–248.

165 J. Buha, D. Arcon, M. Niederberger and I. Djerdj, *Phys. Chem. Chem. Phys.*, 2010, **12**, 15537–15543.

166 H. Kominami, K. Oki, M. Kohno, S.-i. Onoue, Y. Kera and B. Ohtani, *J. Mater. Chem.*, 2001, **11**, 604–609.

167 M. Wei, Z. m. Qi, M. Ichihara and H. Zhou, *Acta Mater.*, 2008, **56**, 2488–2494.

168 W. Hu, Y. Zhao, Z. Liu and Y. Zhu, *Nanotechnology*, 2007, **18**, 095605.

169 H. Luo, M. Wei and K. Wei, *J. Nanomater.*, 2009, **2009**, 758353.

170 S. Kunjara Na Ayudhya, A. Soottitantawat, P. Praserthdam and C. Satayaprasert, *Mater. Chem. Phys.*, 2008, **110**, 387–392.

171 C. C. Li, J. Dou, L. Chen, J. Lin and H. C. Zeng, *ChemCatChem*, 2012, **4**, 1675–1682.

172 L. Fei and X. Dongfeng, *Phys. Scr.*, 2010, **2010**, 014074.

173 H. Wen, Z. Liu, J. Wang, Q. Yang, Y. Li and J. Yu, *Appl. Surf. Sci.*, 2011, **257**, 10084–10088.

174 M. Liu and D. Xue, *Mater. Res. Bull.*, 2010, **45**, 333–338.

175 S. H. Mujawar, A. I. Inamdar, C. A. Betty, V. Ganesan and P. S. Patil, *Electrochim. Acta*, 2007, **52**, 4899–4906.

176 J. Xia, N. Masaki, K. Jiang and S. Yanagida, *J. Photochem. Photobiol., A*, 2007, **188**, 120–127.

177 R. Romero, J. R. Ramos-Barrado, F. Martin and D. Leinen, *Surf. Interface Anal.*, 2004, **36**, 888–891.

178 R. Romero, E. A. Dalchiele, F. Martín, D. Leinen and J. R. Ramos-Barrado, *Sol. Energy Mater. Sol. Cells*, 2009, **93**, 222–229.

179 T. Rajesh, V. Binni, G. M. Subodh, T. Eng Soon and S. Chorng Haur, *Nanotechnology*, 2011, **22**, 115202.

180 J. H. Lim and J. Choi, *J. Ind. Eng. Chem.*, 2009, **15**, 860–864.

181 J. H. Kang, Y. Myung, J. W. Choi, D. M. Jang, C. W. Lee, J. Park and E. H. Cha, *J. Mater. Chem.*, 2012, **22**, 8413–8419.

182 B. Varghese, S. C. Haur and C.-T. Lim, *J. Phys. Chem. C*, 2008, **112**, 10008–10012.

183 R. Kodama, Y. Terada, I. Nakai, S. Komaba and N. Kumagai, *J. Electrochem. Soc.*, 2006, **153**, A583–A588.

184 S. Choopun, N. Hongsith and E. Wongrat, *Metal-Oxide Nanowires by Thermal Oxidation Reaction Technique*, 2010.

185 G. Michael, *J. Photochem. Photobiol., C*, 2003, **4**, 145–153.

186 L. Alibabaei, H. Luo, R. L. House, P. G. Hoertz, R. Lopez and T. J. Meyer, *J. Mater. Chem. A*, 2013, **1**, 4133–4145.

187 R. Jose, V. Thavasi and S. Ramakrishna, *J. Am. Ceram. Soc.*, 2009, **92**, 289–301.

188 K. Sayama, H. Sugihara and H. Arakawa, *Chem. Mater.*, 1998, **10**, 3825–3832.

189 L. Hu, M. Wolf, M. Grätzel and Z. Jiang, *J. Sol-Gel Sci. Technnol.*, 1995, **5**, 219–226.

This journal is © The Royal Society of Chemistry 2014

J. Mater. Chem. A, 2014, **2**, 15683–15703 | **15701**

190 B.-Y. Jeong and E. H. Jung, *Met. Mater. Int.*, 2013, **19**, 617–622.

191 J. Xia, N. Masaki, K. Jiang and S. Yanagida, *Chem. Commun.*, 2007, 138–140.

192 J. Xia, N. Masaki, K. Jiang and S. Yanagida, *J. Phys. Chem. C*, 2007, **111**, 8092–8097.

193 T.-Y. Cho, K.-W. Ko, S.-G. Yoon, S. S. Sekhon, M. G. Kang, Y.-S. Hong and C.-H. Han, *Curr. Appl. Phys.*, 2013, **13**, 1391–1396.

194 J. Kim, *J. Nanosci. Nanotechnol.*, 2011, **11**, 7335–7338.

195 E. Barea, X. Xu, V. Gonzalez-Pedro, T. Ripolles-Sanchis, F. Fabregat-Santiago and J. Bisquert, *Energy Environ. Sci.*, 2011, **4**, 3414–3419.

196 A. Zaban, S. G. Chen, S. Chappel and B. A. Gregg, *Chem. Commun.*, 2000, 2231–2232.

197 S. G. Chen, S. Chappel, Y. Diamant and A. Zaban, *Chem. Mater.*, 2001, **13**, 4629–4634.

198 M. Wu, X. Lin, W. Guo, Y. Wang, L. Chu, T. Ma and K. Wu, *Chem. Commun.*, 2013, **49**, 1058–1060.

199 X. Lin, M. Wu, Y. Wang, A. Hagfeldt and T. Ma, *Chem. Commun.*, 2011, **47**, 11489–11491.

200 M. K. Siddiki, S. Venkatesan and Q. Qiao, *Phys. Chem. Chem. Phys.*, 2012, **14**, 4682–4686.

201 O. Wiranwetchayan, Z. Liang, Q. Zhang, G. Cao and P. Singjai, *Mater. Sci. Appl.*, 2011, **2**, 1697–1701.

202 F. Lenzmann, in *Mesoporous, nanoparticulate films of Nb₂O₅ and ZrO₂ preparation and characterization*, Switzerland, 2000.

203 T. W. Hickmott, *J. Appl. Phys.*, 1966, **37**, 4380–4388.

204 J.-C. Su, C.-L. Lu and C.-W. Chu, *Appl. Opt.*, 2009, **48**, 4942–4946.

205 G. Shen, P.-C. Chen, K. Ryu and C. Zhou, *J. Mater. Chem.*, 2009, **19**, 828–839.

206 N. S. Harale, D. L. Kamble, M. G. Gang, V. K. Rao, J. H. Kim and P. S. Patil, *Mater. Today*, 2013, **16**, 452–453.

207 H. T. H. Kondo, T. Takeuchi and I. Igarashi, *Proc. 3rd Sensor Symp.*, Japan, 1983, pp. 185–190.

208 L. Chambon, C. Maleysson, A. Pauly, J. P. Germain, V. Demarne and A. Grisel, *Sens. Actuators, B*, 1997, **45**, 107–114.

209 L. Chambon, A. Pauly, J. P. Germain, C. Maleysson, V. Demarne and A. Grisel, *Sens. Actuators, B*, 1997, **43**, 60–64.

210 L. Chambon, J. P. Germain, A. Pauly, V. Demarne and A. Grisel, *Sens. Actuators, B*, 1999, **60**, 138–147.

211 R. A. Rani, A. S. Zoolfakar, J. Z. Ou, M. R. Field, M. Austin and K. Kalantar-Zadeh, *Sens. Actuators, B*, 2013, **176**, 149–156.

212 T. Hyodo, J. Ohoka, Y. Shimizu and M. Egashira, *Sens. Actuators, B*, 2006, **117**, 359–366.

213 L. Chevallier, E. Di Bartolomeo, M. L. Grilli, M. Mainas, B. White, E. D. Wachsman and E. Traversa, *Sens. Actuators, B*, 2008, **129**, 591–598.

214 L. Chevallier, E. Di Bartolomeo, M. L. Grilli and E. Traversa, *Sens. Actuators, B*, 2008, **130**, 514–519.

215 H. G. Moon, H. W. Jang, J.-S. Kim, H.-H. Park and S.-J. Yoon, *Sens. Actuators, B*, 2011, **153**, 37–43.

216 T. Hyodo, H. Shibata, Y. Shimizu and M. Egashira, *Sens. Actuators, B*, 2009, **142**, 97–104.

217 A. Kohli, C. C. Wang and S. A. Akbar, *Sens. Actuators, B*, 1999, **56**, 121–128.

218 L. Chevallier, E. Traversa and E. Di Bartolomeo, *J. Electrochem. Soc.*, 2010, **157**, J386–J391.

219 M. S. P. Francisco, W. S. Cardoso and Y. Gushikem, *J. Electroanal. Chem.*, 2005, **574**, 291–297.

220 U. Cvelbar, K. Ostrikov, A. Drenik and M. Mozetic, *Appl. Phys. Lett.*, 2008, **92**, 133505–133503.

221 B. C. Yadav and M. Singh, *IEEE Sens. J.*, 2010, **10**, 1759–1766.

222 O. Korostynska, K. Arshak, E. Gill, A. Arshak and K. Kaneswaran, ″Bi₂O₃/Nb₂O₅ thick film capacitive pH sensor using AD5933 impedance converter″, in *Sensors Applications Symposium, 2008. SAS 2008. IEEE*, 2008, pp. 16–21.

223 J. P. Marco, K. B. Borges, C. R. T. Tarley, E. S. Ribeiro and A. C. Pereira, *J. Electroanal. Chem.*, 2013, **704**, 159–168.

224 S. Rho, D. Jahng, J. H. Lim, J. Choi, J. H. Chang, S. C. Lee and K. J. Kim, *Biosens. Bioelectron.*, 2008, **23**, 852–856.

225 L. Sang, M. Liao and M. Sumiya, *Sensors*, 2013, **13**, 10482–10518.

226 X. Fang, L. Hu, K. Huo, B. Gao, L. Zhao, M. Liao, P. K. Chu, Y. Bando and D. Golberg, *Adv. Funct. Mater.*, 2011, **21**, 3907–3915.

227 V. Etacheri, R. Marom, R. Elazari, G. Salitra and D. Aurbach, *Energy Environ. Sci.*, 2011, **4**, 3243–3262.

228 M. V. Reddy, G. V. Subba Rao and B. V. R. Chowdari, *Chem. Rev.*, 2013, **113**, 5364–5457.

229 K. Naoi, S. Ishimoto, J.-i. Miyamoto and W. Naoi, *Energy Environ. Sci.*, 2012, **5**, 9363–9373.

230 Y. Jing, Z. Zhou, C. R. Cabrera and Z. Chen, *J. Mater. Chem. A*, 2014, **2**, 12104–12122.

231 B. Reichman and A. J. Bard, *J. Electrochem. Soc.*, 1981, **128**, 344–346.

232 N. Kumagai, K. Tanno, T. Nakajima and N. Watanabe, *Electrochim. Acta*, 1983, **28**, 17–22.

233 B. Kaplan, H. Groult, N. Kumagai, S. Komaba and F. Lantelme, *Electrochemistry*, 2001, **69**, 592–597.

234 N. Kumagai, Y. Koishikawa, S. Komaba and N. Koshiba, *J. Electrochem. Soc.*, 1999, **146**, 3203–3210.

235 N. Kumagai, S. Komaba and N. Kumagai, in *New Materials for Batteries and Fuel Cells*, ed. D. H. Doughty, L. F. Nazar, M. Arakawa, H. P. Brack and K. Naoi, 2000, vol. 575, pp. 39–47.

236 N. Kumagai, Y. Tateshita, Y. Takatsuka, M. Baba, T. Ikeda and K. Tanno, *J. Power Sources*, 1995, **54**, 175–179.

237 F. Lantelme, H. Groult and N. Kumagai, *Electrochim. Acta*, 2000, **45**, 3171–3180.

238 H. Nakazawa, K. Sano, T. Abe, M. Baba and N. Kumagai, *J. Power Sources*, 2007, **174**, 838–842.

239 N. Kumagai, I. Ishiyama and K. Tanno, *J. Power Sources*, 1987, **20**, 193–198.

240 M. Wei, K. Wei, M. Ichihara and H. Zhou, *Electrochem. Commun.*, 2008, **10**, 980–983.

241 A. Le Viet, M. V. Reddy, R. Jose, B. V. R. Chowdari and S. Ramakrishna, *Electrochim. Acta*, 2011, **56**, 1518–1528.

242 G. Park, N. Gunawardhana, C. Lee, S.-M. Lee, Y.-S. Lee and M. Yoshio, *J. Power Sources*, 2013, **236**, 145–150.

243 J. W. Kim, V. Augustyn and B. Dunn, *Adv. Energy Mater.*, 2012, **2**, 141–148.

244 V. Augustyn, J. Come, M. A. Lowe, J. W. Kim, P. L. Taberna, S. H. Tolbert, H. D. Abruna, P. Simon and B. Dunn, *Nat. Mater.*, 2013, **12**, 518–522.

245 A. A. Lubimtsev, P. R. C. Kent, B. G. Sumpter and P. Ganesh, *J. Mater. Chem. A*, 2013, **1**, 14951–14956.

246 P.-C. Chen, G. Shen, Y. Shi, H. Chen and C. Zhou, *ACS Nano*, 2010, **4**, 4403–4411.

247 X. Wang, G. Li, Z. Chen, V. Augustyn, X. Ma, G. Wang, B. Dunn and Y. Lu, *Adv. Energy Mater.*, 2011, **1**, 1089–1093.

248 R. H. H. Smits, K. Seshan and J. R. H. Ross, *J. Chem. Soc., Chem. Commun.*, 1991, 558–559.

249 M. I. de Sairre, E. S. Bronze-Uhle and P. M. Donate, *Tetrahedron Lett.*, 2005, **46**, 2705–2708.

250 K. Tanabe, *Catal. Today*, 2003, **78**, 65–77.

251 K. Tanabe and S. Okazaki, *Appl. Catal., A*, 1995, **133**, 191–218.

252 T. Ushikubo, *Catal. Today*, 2000, **57**, 331–338.

253 I. E. Wachs, Y. Chen, J. M. Jehng, L. E. Briand and T. Tanaka, *Catal. Today*, 2003, **78**, 13–24.

254 M. Cherian, M. S. Rao and G. Deo, *Catal. Today*, 2003, **78**, 397–409.

255 M. Ziolek, *Catal. Today*, 2003, **78**, 47–64.

256 F. B. Noronha, D. A. G. Aranda, A. P. Ordine and M. Schmal, *Catal. Today*, 2000, **57**, 275–282.

257 J. M. Jehng, A. M. Turek and I. E. Wachs, *Appl. Catal., A*, 1992, **83**, 179–200.

258 X. Chen, T. Yu, X. Fan, H. Zhang, Z. Li, J. Ye and Z. Zou, *Appl. Surf. Sci.*, 2007, **253**, 8500–8506.

259 H.-Y. Lin, H.-C. Yang and W.-L. Wang, *Catal. Today*, 2011, **174**, 106–113.

260 Y.-H. Pai and S.-Y. Fang, *J. Power Sources*, 2013, **230**, 321–326.

261 S. Qi, R. Zuo, Y. Liu and Y. Wang, *Mater. Res. Bull.*, 2013, **48**, 1213–1217.

262 S. Ge, H. Jia, H. Zhao, Z. Zheng and L. Zhang, *J. Mater. Chem.*, 2010, **20**, 3052–3058.

263 S.-q. Guo, X. Zhang, Z. Zhou, G.-d. Gao and L. Liu, *J. Mater. Chem. A*, 2014, **2**, 9236–9243.

264 R. Baetens, B. P. Jelle and A. Gustavsen, *Sol. Energy Mater. Sol. Cells*, 2010, **94**, 87–105.

265 N. M. Rowley and R. J. Mortimer, *Sci. Prog.*, 2002, **85**, 243–262.

266 J. J. Ho, C. Y. Chen, C. M. Huang, W. J. Lee, W. R. Liou and C. C. Chang, *Appl. Opt.*, 2005, **44**, 6176–6180.

267 S. K. Deb, *Sol. Energy Mater. Sol. Cells*, 2008, **92**, 245–258.

268 S. Heusing, D. L. Sun, J. Otero-Anaya and M. A. Aegerter, *Thin Solid Films*, 2006, **502**, 240–245.

269 C. O. Avellaneda, A. Pawlicka and M. A. Aegerter, *J. Mater. Sci.*, 1998, **33**, 2181–2185.

270 T. Maruyama and T. Kanagawa, *J. Electrochem. Soc.*, 1994, **141**, 2868–2871.

271 N. Ozer and C. M. Lampert, *Sol. Energy Mater. Sol. Cells*, 1998, **54**, 147–156.

272 A. Verma and P. K. Singh, *Indian J. Chem., Sect. A: Inorg., Bioinorg., Phys., Theor. Anal. Chem.*, 2013, **52**, 593–598.

273 A. M. Grishin, A. A. Velichko and A. Jalalian, *Appl. Phys. Lett.*, 2013, **103**, 053111.

274 T. V. Kundozerova, A. M. Grishin, G. B. Stefanovich and A. A. Velichko, *IEEE Trans. Electron Devices*, 2012, **59**, 1144–1148.

275 C.-H. Kao, H. Chen, L.-T. Kuo, J.-C. Wang, Y.-T. Chen, Y.-C. Chu, C.-Y. Chen, C.-S. Lai, S. W. Chang and C. W. Chang, *Sens. Actuators, B*, 2014, **194**, 419–426.